Preparation of N-doped porous carbon materials and their supercapacitor performance

Dissertation Submitted for the Degree of MTech: Engineering: Chemical

Prepared by

Shuang Zong (67136591)

Submitted to Department of Civil and Chemical Engineering, College of Science, Engineering and Technology

University of South Africa

Supervisor(s):

Pro Xinying Liu

Co-supervisor:

Pro Aibing Chen

January 2021

Declarations

I solemnly promise that the content of the paper is all my own real work and it is submitted for a Master's degree in Technologies of Chemical Engineering at the University of South Africa; and this work has not been submitted for any other degree or any other examination to any institution.

On this 27/01/2021 day of 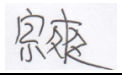

(Candidate)

On this 27/01/2021 day of 

(Supervisor)

On this 27/01/2021 day of 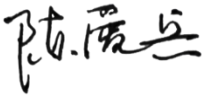

(Co-supervisor)

Abstract

Supercapacitor is the best potential candidate of the energy storage system due to the superior charge or discharge efficiency, high power density (>10 kW kg^{-1}), and long cycling life. Porous carbon materials as the promising electrode material have been widely used in supercapacitor. In fact, conventional porous carbon supercapacitor electrodes cannot fulfil the growing demand of high energy and power densities of supercapacitor. A large number of studies show that nitrogen doping can change the surface electronic structure of carbon materials, thus significantly improving the electrochemical properties. In addition to, the pore structure and morphology of carbon materials have great influence on the electrochemical performance. In this work, we firstly fabricated nitrogen-doped porous carbon nanotubes by using a simple mixed salts ($NaCl/ZnCl_2$) activation strategy. The as-obtained porous carbon nanotubes exhibited excellent electrochemical performance in supercapacitor. Furthermore, two-dimension nitrogen-doping porous nanosheets were prepared by a salt template-assisted monomer deposition method. In this study, by optimizing the synthesis conditions, the as-obtained carbon nanosheets showed a high specific capacitance of 277 F g^{-1} at 1 A g^{-1} and excellent cycle stability retained 91 % after 10,000 cycles.

Key words: porous carbon materials; nitrogen-doping; molten activation; salt template; supercapacitor

Acknowledgements

I am very grateful to the following people for helping me to complete this work:

1. My supervisor, Prof Xinying Liu, for helping me to revise the dissertation and experiment with ideas, and for helping me with school affairs.
2. My co-supervisor, Prof Aibing Chen, for allowing me to use the lab for my experiment, giving me time off to do my research and to write the dissertation, and for encouraging me to further my studies.
3. PhD students at IDEAS UNISA, Mr Yusheng Zhang, Mr Jianqi Shen, Mr Jianli Chang for helping me with school affairs.
4. UNISA and Hebei University of Science & Technology for funding my studies.

I also thank my entire family for encouraging and supporting me; I would not have done it without all of your support.

List of Publications

[1] Wu H, Qin Y, **Zong S**, Hu Y, Xaba M. S, Liu X, Chen A. Porous yolk-shell-structured carbon nanospheres for electrochemical energy storage. Journal of Materials Science: Materials in Electronics, 2020, 31(16):13321-13329.

[2] **Zong S**, Liu X, Chen A. Metal-organic frameworks-derived zero-dimensional materials for supercapacitors. CIESC Journal. 2020, 71 (6): 2612-2627.

[3] **Zong S**, Zhang Y, Xaba M. S, Liu X, Chen A. N-doped porous carbon nanotubes derived from polypyrrole for supercapacitors with high performance. J. Anal. Appl. Pyrolysis. 2020, 152, 104925.

[4] Wang W, Liu L, **Zong S**, Chen A. Nitrogen-doped hollow mesoporous carbon tube for supercapacitors application. Journal of the Electrochemical Society. 2019, 166 (16): A404-A4055.

[5] Du J, **Zong S**, Zhang Y, Hou S, Chen A. Co-assembly strategy for uniform and tunable hollow carbon spheres with supercapacitor application. Journal of Colloid and Interface Science. 2020, 565: 245-253.

[6] Du. J, Chen. A, **Zong S**, Zhang Y, Wu H, Liu L. PVP-assisted preparation of nitrogen doped mesoporous carbon materials for supercapacitors. Journal of Materials Science & Technology. 2020, 58: 197-204.

Table of Contents

The List of Figures

List of Tables

List of Abbreviations and Symbols

BET:	Brunnauer-Emmett-Teller
CV:	cyclic voltammetry
CVD:	chemical vapor deposition
EDLC:	electrochemical double-layer capacitors
EIS:	electrical impedance spectroscopy
ESD:	energy storage devices
FTIR:	Fourier transform infrared spectroscopy
GCD:	galvanostatic charge-discharge
CTAB:	cetyltrimethylammonium bromide
APS:	ammonium persulfate
NCNs-A:	N-doped porous carbon nanotubes
NPC:	nitrogen-doped porous carbon
PCNs:	porous carbon nanotubes
PPy:	polypyrrole
SEM:	scanning electron microscope
SSA:	specific surface area
TEM:	transmission electron microscope
XPS:	X-ray photoelectron spectroscopy
XRD:	X-ray diffraction

CHAPTER 1

Introduction

1.1 Background

With the rapid development of the global economy, energy consumption is accelerating at an alarming rate. Owing to the excessive use of energy and the large amount of greenhouse gas emission, the world is facing energy crises and a number of urgent environmental issues.[1–4] The development and utilization of sustainable energy has become a hotspot of research. In recent years, the reasonable utilization of renewable energy such as wind, solar, tidal, and biomass energy have shown a positive trend.[5,6] However, owing to the impact of the environment, the forms of these energy sources are intermittent. Proper storage and transmission are needed to make full use of these energy sources; as a result, the actual situation has caused some limitations in their use. Therefore, the exploitation of new energy conversion and storage devices that are an alternative energy source to achieve clean and sustainable development has become an important research direction. A series of energy storage devices (ESD) emerged at the right moment: for example, rechargeable batteries, supercapacitors and fuel cells, which are considered an important part of energy storage technology. Among these ESD, supercapacitors, due to their significantly long cycling life, higher power density, shorter charge-discharge time, wide operating temperature, and green environmental protection, have been regarded as one of the most promising ESD.[7–11]

Supercapacitors' electrochemical performance is closely related to that of electrode

materials. An excellent electrochemical performance electrode material is characterized by high conductivity, a large specific surface area (SSA), a distribution of pores with optimized size, good corrosion resistance, etc.[12-16] Therefore, the selection of suitable materials and the optimal design of electrode materials are key strategies for making supercapacitors more efficient than other ESD, such as batteries.[17,18]

1.2 Problem Statement

In recent years, numerous materials have been used as electrode materials for supercapacitors. Carbon material (activated carbon, carbon nanotubes, graphene, etc.)[19] have the characteristics of good electrical conductivity, high SSA, stable chemical properties, long cycle stability, and a long service life, which makes these the most promising materials for supercapacitors. Theoretically, the high SSA of carbon materials and the low positive and negative charge spacing make their specific capacitance values much greater than those of traditional capacitors. But, in fact, the energy storage capacity is not ideal, because: (1) the surface of carbon material is not an ideal plane - it is uneven and usually has a certain degree of arcing: after the ions are arranged on the surface of the carbon material, which lead the electric double layer presents a curved interface;[20] (2) the distance between adjacent carbon walls in the pores of the materials is too small, resulting in the electric double layer formed in between being directly combined into an ion layer; (3) the electrochemical double-layer capacitors (EDLC) performance is affected by the pore size and the channel shape of carbon materials, as well as the wettability and conductivity of carbon materials during

the discharge process.[21] Therefore, the application of carbon materials in supercapacitors warrants further study.

1.3 Research Aims

Carbon materials mainly depend on the contact transfer charge between the interface and the electrolyte to generate capacitance in supercapacitors. A high specific surface area (SSA) to ensure the space for charge storage and thus the capacitance performance of carbon materials can be improved by increasing the specific surface area. And by modifying the surface characteristics of the carbon materials (such as doping N atoms), the conductivity and wettability of the materials can be improved, in this way enhancing the capacitance of the supercapacitors. Above of this, this project will seek to determine the following:

1.3.1 Focusing on the morphology, structure and chemical composition of carbon materials, with the goal of improving the capacitance performance of carbon materials, seeking appropriate synthesis strategy to synthesize carbon materials with specific morphology and structure.

1.3.2 Selecting suitable characterization methods to characterize the as-obtained carbon materials, and investigating their electrochemical performance in supercapacitors, in order to study the interaction between the carrier and the resultant activity.

1.4 Dissertation Overview

The dissertation consists of six chapters. Chapter 1 includes four parts: research

background, current problem statement, research objectives and a brief introduction of the dissertation outline.

Chapter 2 introduces the relevant background of this research topic, which summarizes the relevant research work in the literature to highlight that our research topic can provide a proposition for the development of electrode materials in high-performance supercapacitors.

Chapter 3 is an introduction to the reagents, equipment, and characterization methods used in the dissertation.

Chapter 4 demonstrates the N-doped porous carbon nanotubes (NCNs-A) which were prepared by a simple strategy of mixed salts ($NaCl/ZnCl_2$) activation with polypyrrole (PPy) as a carbon precursor. In this process, mixed salts $NaCl/ZnCl_2$ were utilized as a porogen-template to create abundant pores and simultaneously act as supporting template to maintain the tubular-like morphology from PPy. In addition, the effect factors on the electrochemical performance of the NCNs-A is discussed. These results indicate that optimal synthesis conditions are the mixed salts mass ratio of 2 and the carbonization temperature at 800 ℃. When used as electrode material for supercapacitors, the NCNs-A exhibited outstanding electrochemical performance.

Chapter 5 details a “salt template”-assisted monomer deposition strategy to synthesize

nitrogen-doped porous carbon (NPC) in which sodium chloride (NaCl) crystal was used as a salt template, 3-aminophenol as carbon and nitrogen precursor, and the transition metal salt cobalt nitrate hexahydrate as a catalyst. Scanning electron microscopy showed the obtained NPC to have a large pore structure. Nitrogen adsorption–desorption isothermals were used to ensure the pore structures of NPC. The prepared NPC with large SSA and appropriate N-doping displays outstanding electrochemical performance as electrode materials in supercapacitors.

Chapter 6 summarizes the main research content of this dissertation and puts forward some views on the research results of this topic.

References

[1] Winter M, and Brodd R J. What are batteries, fuel cells, and supercapacitors. Chemical Reviews. 2004, 104(10): 4245-4269.

[2] Islam M S, and Fisher C A J. Lithium and sodium battery cathode materials: computational insights into voltage, diffusion and nanostructural properties. Chemical Society Reviews. 2014, 43(1): 185-204.

[3] Wang Q, Yan J, and Fan Z. Carbon materials for high volumetric performance supercapacitors: design, progress, challenges and opportunities. Energy & Environmental Science. 2016, 9(3): 729-762.

[4] Zhang Q, Zhao B, Wang J, Qu C, Sun H, Zhang K, and Liu M. High-performance hybrid supercapacitors based on self-supported 3D ultrathin porous quaternary Zn-Ni-Al-Co oxide nanosheets. Nano Energy. 2016, 28: 475-485.

[5] Liu C F, Liu Y C, Yi T Y, and Hu C C. Carbon materials for high-voltage supercapacitors. Carbon. 2019, 145: 529-548.

[6] Badenhorst H. A review of the application of carbon materials in solar thermal energy storage. Solar Energy. 2019, 192: 35-68.

[7] Guo N, Li M, Sun X, Wang F, and Yang R. Enzymatic hydrolysis lignin derived hierarchical porous carbon for supercapacitors in ionic liquids with high power and energy densities. Green Chemistry. 2017, 19(11): 2595-2602.

[8] Sheberla D, Bachman J C, Elias J S, Sun C J, Yang S H, and Dincă M. Conductive MOF electrodes for stable supercapacitors with high areal capacitance. Nature materials. 2017, 16(2): 220-224.

[9] Qu L, Zhao Y, Khan A M, Han C H, Hercule K M, Yan M Y, Liu X Y, Chen W, Wang D D, Cai Z Y, Xu W W, Zhao K N, Zheng X L, and Mai L Q. Interwoven three-dimensional architecture of cobalt oxide nanobrush-graphene@$Ni_xCo_2x(OH)_{6x}$ for high-performance supercapacitors. Nano letters. 2015, 15(3): 2037-2044.

[10] Mackanic, David G, Chang T H, Huang Z J, Cui Y, and Bao Z N. Stretchable electrochemical energy storage devices. Chem. Soc. Rev. 2020, 49: 4466-4495.

[11] Cossutta M, Vretenar V, Centeno T A, Kotruszd Peter, McKechnieaet J, and Pickeringe S J. A comparative life cycle assessment of graphene and activated carbon in a supercapacitor application. Journal of Cleaner Production. 2020, 242: 118468.

[12] Chmiola J, Largeot C, Taberna P L, Simon P, and Gogotsi Y. Monolithic carbide-derived carbon films for micro-supercapacitors. Science. 2010, 328(5977): 480-483.

[13] Zeng L, Lou X, Zhang J, Wu C, Liu J, and Jia C K. Carbonaceous mudstone and lignin-derived activated carbon and its application for supercapacitor electrode. Surface and Coatings Technology. 2019, 357: 580-586.

[14] Pech D, Brunet M, Durou H, Huang P H, Mochalin V, Gogotsi Y, Taberna P L, and Simon P. Ultrahigh-power micrometre-sized supercapacitors based on onion-like carbon. Nature nanotechnology. 2010, 5(9): 651-654.

[15] He Y, Chen W, Li X, Zhang Z X, Fu J C, Zhao C H, and Xie E Q. Freestanding three-dimensional graphene/MnO_2 composite networks as ultralight and flexible

supercapacitor electrodes. ACS Nano. 2013, 7(1): 174-182.

[16] Wan L, Wei W, Xie M, Zhang Y, Li X, Xiao R, Chen J, and Du C. Nitrogen, sulfur co-doped hierarchically porous carbon from rape pollen as high-performance supercapacitor electrode. Electrochimica Acta. 2019, 311: 72-82.

[17] Song Z, and Zhou H. Towards sustainable and versatile energy storage devices: an overview of organic electrode materials. Energy & Environmental Science. 2013, 6(8): 2280-2301.

[18] González A, Goikolea E, Barrena J A, and Mysyk R. Review on supercapacitors: Technologies and materials. Renewable and Sustainable Energy Reviews. 2016, 58: 1189-1206.

[19] Yang Z, Tian J, Yin Z, Cui C J, Qian W Z, and Wei F. Carbon nanotube- and graphene-based nanomaterials and applications in high-voltage supercapacitor: A review. Carbon. 2019, 141: 467-480.

[20] Huang J, Sumpter B, and Meunier V. Theoretical model for nanoporous carbon supercapacitors. Angew Chem. Int. Ed. Engl. 2010, 47(3): 520-524.

[21] Ciszewski M, Koszorek A, Radko T, Szatkowski P, and Janas D. Review of the selected carbon-based materials for symmetric supercapacitor application. Journal of Electronic Material, 2019, 48(2): 717-744.

CHAPTER 2

Literature Review

2.1 Introduction to Supercapacitors

Energy resource shortages and environmental pollution problems which are caused by the consumption of fossil fuels have attracted considerable attention. Vigorously developing energy storage and conversion equipment is an effective way to solve these limitations.[1,2] Owing to the rapid charge–discharge, high power densities, and long energy storage capacity, supercapacitors, as the most promising energy storage devices, have experienced a significant increase in application during the past few decades.[3]

As early as in 1879, the interface electric double-layer phenomenon was discovered by Helmholtz and then he proposed the concept of the electric double layer.[4] With supercapacitors, also known as electrochemical capacitors, unlike other ESD (for instance fuel cells and batteries), charge storage occurs in a double-layered electrical layer which is formed at the interface between electrode and electrolyte. Currently, supercapacitors are widely used in memory backup systems, electronics, and industrial energy/power management equipment. One of the most notable recent applications of supercapacitors is in the emergency doors of the Airbus A380.[5] More recently, Shanghai Aowei Technology Co. Ltd (China) and the Chinese CSR Co. Ltd have been using supercapacitors for trolley buses and electric tramcars, respectively.[6] These examples fully indicate the reliability and safety of the new-era supercapacitors in practical applications.[7,8]

2.2 Energy Storage Mechanism of Supercapacitors

Based on two different storage mechanisms, there are two types of supercapacitor, which consist of EDLC and pseudo-capacitors. EDLC physically store charge in a double Helmholtz layer by reversible ion adsorption,[9] and it is shown in Fig. 2.1 below:

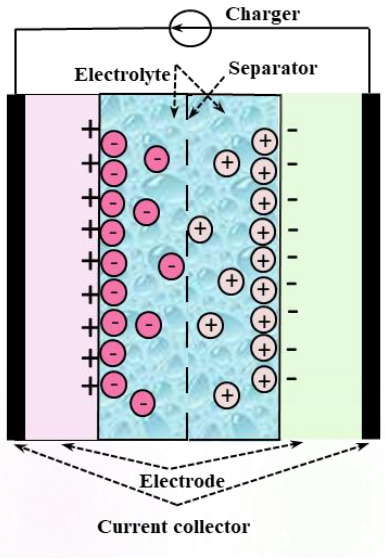

Fig. 2.1: Schematic of operating principle of EDLC

When the capacitor is charged, a large amount of positive charge is collected on the positive plate; at the same time, a large amount of negative charge will be collected on the negative plate. When the electrode is put into the electrolyte, there will be a quantitative excess of positively and negatively charged layers between its surface and the electrolyte. As a result, a certain potential difference is formed between the two charge layers. Under the action of coulomb force and inter-molecular (ion) force, due to the attraction, the anions (cations) in the electrolyte will move to the surface of positive (negative) charges. At the same time, a certain barrier will be formed between the positive and negative charges, leading to the charges between the two charge layers that cannot be crossed to achieve neutrality, thereby forming a dense double charge.

When the capacitor is discharged, the electrons flow by the external circuit from the negative charge layer to the positive charge layer, and the potential of the electrode surface is quickly restored. The cation and anion accumulated on the electrode surface quickly return to the electrolyte from the electrode surface. During the entire charging and discharging process, no electrochemical reaction occurs between the electrode and the electrolyte, only the simple physical adsorption and desorption process of electrons. Research shows that the concentration of the electrolyte does not change, and energy storage and release occur only at the interface of the electric double layer during the charge and discharge processes. This shows convincingly that EDLC possesses the advantages of good cycle performance, long service life, and high safety performance, etc.[10,11]

Differently from EDLC, a pseudocapacitor relies on an under-potential deposition on two-dimensional or three-dimensional space on the electrode surface or bulk phase, and on energy storage through reversible chemisorption and redox reactions. The charging and discharging mechanism is as follows: when the pseudocapacitor is charged, under an external electric field, those ions in electrolyte diffuse from the solution to the interface between electrode and electrolyte. Then surface active materials enter the electrode through the electrochemical reaction at the interface, storing charges in the electrode. Through ion orientation and control of the charge transfer rate, charge transfer can occur in a relatively short time, resulting in higher capacitance and energy density. In the discharge process, the charge accumulated on the electrode surface is

returned to the electrolyte solution. For pseudocapacitors, the electrode materials usually involved in transition are metal oxides (such as RuO_2, MnO_2, NiO, Fe_2O_3, etc.)[12,13] and conducting polymers (e.g. polypyrrole, polyaniline).[14] Generally, for supercapacitors, two types of energy storage method for EDLC and pseudocapacitors exist at the same time. In different environments, one mechanism will dominate and the other one will be relatively subordinate.

2.3 Electrode Materials for Supercapacitors

Electrode materials as one of the critical factors for supercapacitors, play vital role in the development of supercapacitors. They generally include three types: carbon materials, metal compounds[15,16] and conductive polymers.[17-19]

2.3.1 Carbon Materials

Carbon materials, especially porous carbon nano-materials due to their high SSA, rich pore structure, adjustable pore size, good corrosion resistance, heat resistance, and strong electrical conductivity are being more and more widely used in adsorption, catalysis and other fields.[20,21] It is generally assumed that micropores in carbon materials can significantly increase the SSA of carbon materials and this is vital for enhancing capacitance. Nevertheless, the intricate microporous structure of carbon materials is not always conducive to the improvement of capacitance. As is well known, ultra-micropores (< 0.70 nm) can generate higher capacitance values through solvent deionization at relatively lower current densities, but these pores are not easily

accessible at high discharge rates, resulting in relatively poor capacitance.[22] In other words, the size of capacitors depends on the reachable surface area of carbon materials, and the release behavior of the capacitor is related to the pore structure of carbon materials. It follows that optimizing the pore structure of electrode materials is a prerequisite to improving the capacitance of supercapacitors.

Moreover, typically according to different dimensions, carbon materials can be classified into zero dimension (0D), for example, fullerene, quantum dots, and nanoparticles;[23,24] one dimension (1D), for example, nanofibers, nanowires, nanotubes, and nanobelts;[25,26] two dimension (2D), for example, grapheme and other layered van der Waals solids such as MoS_2;[27,28] and three dimension (3D) assemblies of CNT and graphene, mesoporous carbon, and graphene aerogel, etc.[29,30] Fig. 2.2 summarizes the electrode materials from 0D to 3D.

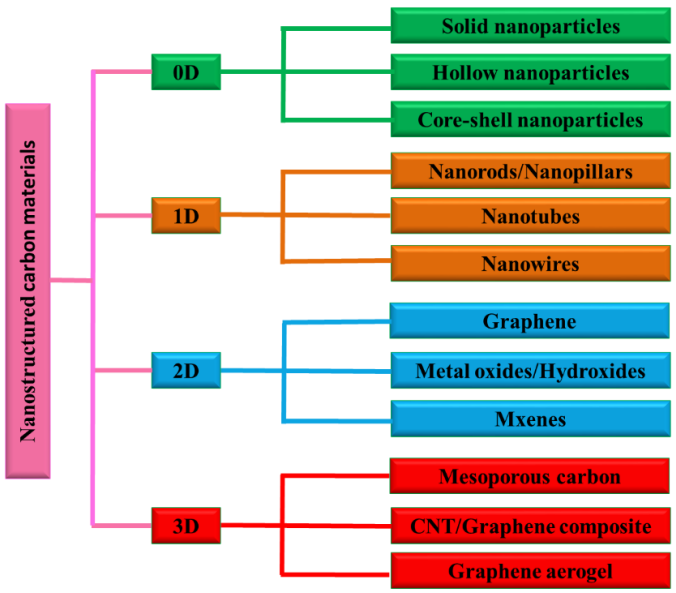

Fig. 2.2: Different dimensions of nanostructured carbon materials

As is well known, the criteria that design high-performance supercapacitor electrodes

include: high specific capacitance (the energy storage per unit volume, mass and area of materials), large rate capability (high capacitance retention under high scan rates), and high cycling stability. Certainly, synthetic cost and environmental friendliness are two important factors that should also be considered in electrode design. Despite the rapid development of carbon materials in recent years, further efforts have been needed to develop superior-performance electrode materials for supercapacitors.

2.3.2 Metal Compounds

Metal compounds are important kinds of electrode materials that possess high energy density and favorable stability compared to other kinds of carbon materials. These have become a research focus in the field of supercapacitors. Among many metal compounds, metal oxide materials have been known as promising candidates to be used as electrodes in supercapacitors due to their abundant reserves, environmental geniality and other intriguing characteristics.[31,32] They are mainly redox reactions that occur at the interface between electrode and electrolyte solution, and they produce a higher capacitance than electric double layers. The most representative of these is the RuO_2; however, because of high cost factors, people are forced to seek alternative materials that are low-cost, environmentally friendly, and are capable of excellent performance. Alternative materials such as MnO_2 and Co_3O_4 have become hot research topics.[33,34] MnO_2 is an ideal supercapacitor electrode material due to its abundant sources and environmental friendliness, but compared to RuO_2, its low conductivity and large internal resistance, the actual specific capacitance is not ideal. How to improve the

conductivity of MnO_2, reduce the internal resistance, and improve its electrochemical performance is the focus of the research.

In addition to the aforementioned metal oxides, bimetal oxides[35] and composites of metal oxides and other materials[36] have been reported on successively in recent years. By adjusting and controlling metal oxides' defects and surfaces/interfaces under a certain nanoscale, the study of functional metal oxide materials with excellent electrochemical performance has become imperative.[37]

2.3.3 Conductive Polymers

Conductive polymers have the advantages of low cost, high voltage window, high theoretical capacity, specific energy and specific power, so they are very suitable as electrode materials for supercapacitors. A conductive polymer realizes energy storage through redox reactions. In the process, the ions in the electrolyte continue to undergo the process of transference from the electrolyte to the polymer skeleton and detachment from the skeleton into the electrolyte. Many researchers have reported on the common conducting polymers, such as PANI and PPy, which are the most promising compounds with low cost, environmental stability and a facile synthesis route.[38-40] However, during the process of ionic insertion and detachment in the electrolyte, the polymer will undergo volume expansion or contraction to varying degrees, resulting in poor electrode material stability. In future, the research directions should focus on improving chemical structure, conductivity, and the stability of conductive polymers to improve

their cycle stability.

2.4 Conclusion

In a word, electrode material is critical factor to the electrochemical performance of supercapacitors. Carbon materials are the most promising electrode material for supercapacitor, contributing to their large specific surface area, high electrical conductivity and extraordinary cycling stability.[41-43] As electrode materials in supercapacitors, the morphologies, pore structure distribution, and surface properties of carbon materials have very important effects on electrochemical performance. Although the currently reported-on materials have made some progress in supercapacitor development, there are still some challenges in the development of carbon materials with good rate performance, supernal energy densities, and stable cycling performance. We hope, through the relevant research and exploration of this topic, to develop the facile, scalable, and green synthesis process to prepare carbon materials for supercapacitors.

References

[1] Shi Y, Peng L, Ding Y, Zhao Y, and Yu G H. Nanostructured conductive polymers for advanced energy storage. Chemical Society Reviews. 2015, 44(19): 6684-6696.

[2] Xie Q X, Bao R R, Zheng A R, Zhang Y F, Wu S H, Xie C, and Zhao P. Sustainable low-cost green electrodes with high volumetric capacitance for aqueous symmetric supercapacitors with high energy density. ACS Sustainable Chemistry & Engineering. 2016, 4(3): 1422-1430.

[3] Borenstein A, Hanna O, Attias R, Luski S, Brousse T, and Aurbach D. Carbon-based composite materials for supercapacitor electrodes: a review. Journal of Materials Chemistry A. 2017, 5(25): 12653-12672.

[4] Helmholtz H. Ueber Einige Gesetze der Vertheilung Elektrischer Ströme in Körperlichen Leitern mit Anwendung auf die Thierisch-Elektrischen Versuche. Ann. Phys. Chem. 1853, 89: 211-233.

[5] Simon P, and Gogotsi Y. Capacitive energy storage in nanostructured carbon-electrolyte systems. Accounts of Chemical Research. 2013, 46(5): 1094-1103.

[6] Wang Y, Song Y, and Xia Y. Electrochemical capacitors: mechanism, materials, systems, characterization and applications. Chemical Society Reviews. 2016, 45(21): 5925-5950.

[7] Lokhande C D, Dubal D P, and Joo O S. Metal oxide thin film-based supercapacitors. Current Applied Physics. 2011, 11(3): 255-270.

[8] Jiang H, Yang L P, Li C Z, Yan C Y, Lee P S, and Ma J. High-rate electrochemical capacitors from highly graphitic carbon-tipped manganese oxide/mesoporous

carbon/manganese oxide hybrid nanowires. Energy and Environmental Science. 2011, 4(5): 1813-1819.

[9] Conway B E. Electrochemical supercapacitors: Scientific fundamentals and technological applications. Springer Science and Business Media. 1999, 481-505.

[10] Sheng J, Ma C, Ma Y, Zhang H X, Wang R R, Xie Z Y, and Shi J L. Synthesis of microporous carbon nanofibers with high specific surface using tetraethyl orthosilicate template for supercapacitors. International Journal of Hydrogen Energy. 2016, 41(22): 9383-9393.

[11] Liu C F, Liu Y C, Yi T Y, and Hu C C. Carbon materials for high-voltage supercapacitors. Carbon. 2019, 145: 529-548.

[12] Liu Q, Yang J J, Luo X G, Miao Y F, Zhang Y, Xu W T, Yang L J, Liang Y X, Weng W, and Zhu M F. Fabrication of a fibrous MnO_2@MXene/CNT electrode for high-performance flexible supercapacitor. Ceramics International. 2020, 46(8): 11874-11881.

[13] Shang Y Z, Ma S, Wei Y M, Yang H, and Xu Z L. Flower-like ternary metal of Ni-Co-Mn hydroxide combined with carbon nanotube for supercapacitor. Ionics. 2020, 26: 3609-3619.

[14] Yanilmaz M, Dirican M, Asiri A M, and Zhang X W. Flexible polyaniline-carbon nanofiber supercapacitor electrodes. Journal of Energy Storage. 2019, 24: 100766.

[15] Kou T Y, Yao B, Liu T Y, and Li Y. Recent advances in chemical methods for activating carbon and metal oxide-based electrodes for supercapacitors. Journal of Materials Chemistry. 2017, 5(33): 17151-17173.

[16] Lao Z. J., Konstantinov K., Tournaire Y., Ng S. H., Wang G. X., and Liu H. K. Synthesis of vanadium pentoxide powders with enhanced surface-area for electrochemical capacitors. Journal of power sources. 2006, 162(2): 1451-1454.

[17] Ma Y, Hou C P, Zhang H P, Zhang Q Y, Liu H, Wu S, and Guo Z H. Three-dimensional core-shell Fe_3O_4/Polyaniline coaxial heterogeneous nanonets: Preparation and high-performance supercapacitor electrodes. Electrochimica Acta. 2019, 315: 114-123.

[18] Herou S, Ribadeneyra M C, Madhu R, Araullo-Peters V, Jensen A, Schlee P and Titirici M. Ordered mesoporous carbons from lignin: A new class of biobased electrodes for supercapacitors. Green chemistry. 2019, 21(3): 550-559.

[19] Liu P, Yang M Y, Zhou S H, Huang Y, and Zhu Y. Hierarchical shell-core structures of concave spherical NiO nanospines@ carbon for high performance supercapacitor electrodes. Electrochimica Acta. 2019, 294: 383-390.

[20] Wang Q, Yan J, Wei T, Feng J, Ren Y M, Fan Z J, Zhang M L, and Jing X Y. Two-dimensional mesoporous carbon sheet-like framework material for high-rate supercapacitors. Carbon. 2013, 60: 481-487.

[21] Fan Y, Yang X, Zhu B, Liu P F, and Lu H T. Micro-mesoporous carbon spheres derived from carrageenan as electrode material for supercapacitors. Journal of Power Sources. 2014, 268: 584-590.

[22] Kang D M, Liu Q L, Gu J J, Su Y S, Zhang W, and Zhang D. “Egg-Box”-assisted fabrication of porous carbon with small mesopores for high-rate electric double layer capacitors. ACS Nano. 2015, 9(11): 11225-11233.

[23] Zhang Q L, O'Brien S C, Heath J R, Liu Y, Curl R F, Kroto H W, and Smalley R E. Reactivity of large carbon clusters: spheroidal carbon shells and their possible relevance to the formation and morphology of soot. The Journal of Physical Chemistry. 1986, 90(4): 525-528.

[24] Dai L M, Chang D W, Baek J B, and Lu W. Carbon nanomaterials for advanced energy conversion and storage. Small. 2012, 8(8): 1130-1166.

[25] Xie C, Yang S H, Xu X Q, Shi J W, and Niu C M. Core-shell structured carbon nanotubes/N-doped carbon layer nanocomposites for supercapacitor electrodes. Journal of Nanoparticle Research. 2020, 22(1): 25.

[26] Deka B K, Hazarika A, Kim J, Kim N, Jeong H E, Park Y B, and Park H W. Bimetallic copper cobalt selenide nanowire-anchored woven carbon fiber-based structural supercapacitors. Chemical Engineering Journal. 2019, 355: 551-559.

[27] Yu J H, Cui Z X, Li X, Chen D, Ji J W, Zhang Q, Sui J, Yu L Y and Dong L F. Facile fabrication of ZIF-derived graphene-based 2D Zn/Co oxide hybrid for high-performance supercapacitors. Journal of Energy Storage. 2020, 27: 101165.

[28] Chen W S, Yu X, Zhao Z X, Ji S C, and Feng L G. Hierarchical architecture of coupling graphene and 2D WS_2 for high-performance supercapacitor. Electrochimica Acta. 2019, 298: 313-320.

[29] Yuan Y, Lv H P, Xu Q J, Liu H M, and Wang Y G. A few-layered MoS_2 nanosheets/nitrogen-doped graphene 3D aerogel as a high performance and long-term stability supercapacitor electrode. Nanoscale. 2019, 11(10): 4318-4327.

[30] Li B L, Li Z S, Pang Q, Zhuang Q T, Zhu J L, Tsiakaras P, and Shen P K. Synthesis

and characterization of activated 3D graphene via catalytic growth and chemical activation for electrochemical energy storage in supercapacitors. Electrochimica Acta. 2019, 324: 134878.

[31] Wang G P, Zhang L, and Zhang J J. A review of electrode materials for electrochemical supercapacitors. Chemical Society Reviews. 2012, 41(2): 797-828.

[32] Lu Q, Chen J G, and Xiao J Q. Nanostructured electrodes for high-performance pseudocapacitors. Angewandte Chemie International Edition. 2013, 52(7): 1882-1889.

[33] Yu G H, Hu L B, Liu N, Wang H L, Vosgueritchian M, Yang Y, Cui Y, and Bao Z N. Enhancing the supercapacitor performance of graphene/MnO_2 nanostructured electrodes by conductive wrapping. Nano Letters. 2011, 11(10): 4438-4442.

[34] Bao L, Li T, Chen S, Peng C, Li L, Xu Q, Chen Y S, Qu E C, and Xu W J. 3D graphene frameworks/Co_3O_4 composites electrode for high-performance supercapacitor and enzymeless glucose detection. Small. 2017, 13(5): 1602077.

[35] Zhang Y F, Li L Q, Su H Q, Huang W, and Dong X C. Binary metal oxide: advanced energy storage materials in supercapacitors. Journal of Materials Chemistry A. 2015, 3(1): 43-59.

[36] Zou R, Quan H Y, Pan M H, Zhou S, Chen D Z, and Luo X B. Self-assembled MXene (Ti_3C_2Tx)/α-Fe_2O_3 nanocomposite as negative electrode material for supercapacitors. Electrochimica Acta. 2018, 292: 31-38.

[37] Lu X F, Wang C, Favier F, and Pinna N. Electrospun nanomaterials for supercapacitor electrodes: Designed architectures and electrochemical

performance. Advanced Energy Materials. 2017, 7(2): 1601301.

[38] Wang H H, Lin J Y, and Shen Z X. Polyaniline (PANI) based electrode materials for energy storage and conversion. Journal of Science: Advanced Materials and Devices. 2016, 1(3): 225-255.

[39] Yang L J, Shi M J, Jiang J T, Liu Y C, Yan C, Liu H, and Guo Z H. Heterogeneous interface induced formation of balsam pear-like PPy for high performance supercapacitors. Materials Letters. 2019, 244: 27-30.

[40] Inamdar A I, Chavan H S, Kim H, and Im H. Mesoporous Ni-PANI composite electrode for electrochromic energy storage applications. Solar Energy Materials and Solar Cells. 2019, 201: 110121.

[41] You B, Yang J, Sun Y Q, and Su Q D. Easy synthesis of hollow core, bimodal mesoporous shell carbon nanospheres and their application in supercapacitor. Chemical Communications. 2011, 47(45): 12364-12366.

[42] Wang Y L, Dong S Y, Wu X Q, Liu X W, and Li M G. Core-shell N-doped carbon spheres for high-performance supercapacitors. Journal of Materials Science. 2017, 52(16): 9673-9682.

[43] Song Y F, Yang J, Wang K, Haller S, Wang Y G, Wang C X, and Xia Y Y. In-situ synthesis of graphene/nitrogen-doped ordered mesoporous carbon nanosheet for supercapacitor application. Carbon. 2016, 96: 955-964.

CHAPTER 3

Experimental: Chemical Reagents, Instruments and Characterization Methods

3.1 Reagents and Instruments

The chemical reagents used in this study are tabulated in Table 3.1

Table 3.1: Chemical reagents

Name	Molecular formula	Grade	Supplier
Zinc chloride	$ZnCl_2$	AR	Tianjin Yongda Chemical Corp
Sodium chloride	NaCl	AR	Tianjin Yongda Chemical Corp
Pyrrole	C_4H_5N	AR 99 %	Aladdin Corp
Cetyltrimethylammonium bromide	$C_{16}H_{33}(CH_3)_3NBr$	AR	Shanghai Fujie Chemical Corp
Hydrochloric acid	HCl	AR 36 wt%	Tianjin Yongda Chemical Corp
Ammonium persulfate	$(NH_4)_2S_2O_8$	AR	Kemi Ou Chemical Corp
3-Aminophenol	C_6H_7NO	AR	Aladdin Corp
Cobalt nitrate hexahydrate	$Co(NO_3)_2$ ·$6H_2O$	AR	Aladdin Corp
Nitrogen	N_2	99.999%	Xisanjiao gas Co., Ltd

All reagents were used as received. All experiments used deionized water as a solvent medium, with a conductivity of 18.2 MΩ cm.

The instruments involved in this study are listed in the table below:

Table 3.2: Experimental instruments

Instrument name	Specification	Supplier
Freezing Dryer	SC21CL	Biocool Co., Ltd
Electronic Balance	AR1510	Ohous Co., Ltd
Centrifuge	H1650	Hunan xiangyi experimental instrument Co., Ltd
Tube Furnace	SRJK-2-13A	Shenyang Energy-saving Electric Furnace Co., Ltd
Transmission Electron Microscope	JEOL JEM-2100	Jeol Co., Ltd
X-ray Photoelectron Spectrometer	ESCALab250Xi	Thermo Co., Ltd
X-ray Diffractometer	Rigaku D/MAX-2500	Rigaku Co., Ltd
Scanning Electron Microscope	S4800I	Hitachi co., Ltd
Fourier Transform Infrared Spectrophotometer	Thermo Nicolet 6700	Thermo
Brunauer-Emmett-Teller surface area analyser	Tristar 3020	Micromeritics Co., Ltd
Electrochemical Workstation	CHI760	Shanghaihuachen Co., Ltd

3.2 Materials Synthesis

Material synthesis is detailed in each chapter.

3.3 The Characterization of Materials

The prepared samples were characterized by Fourier Transform Infrared Spectroscopy (FTIR), X-ray Diffraction (XRD), Transmission Electron Microscope (TEM), Scanning Electron Microscope (SEM), X-ray Photoelectron Spectroscopy (XPS), Brunauer-Emmett-Teller (BET) to analyze their properties and morphology.

3.3.1 Scanning Electron Microscope

In this dissertation, the overall morphology of the microcosmic surface of all samples was observed by means of an S4800I electron microscope in HITACHI, Japan.

1) Sample preparation: The samples to be tested are placed on the sample stage with conductive adhesive, and the test is started after gold spraying treatment.

2) Test condition: During the test process, the acceleration voltage of the instrument is 3 kV, the electron current intensity is 20 keV, and the magnification is 200-70.0 K.

3.3.2 Transmission Electron Microscopy

The structure of the obtained samples was characterized using a transmission electron microscope (TEM, JEOL JEM-2100) with an accelerating voltage of 200 kV.

Sample preparation: A small amount of sample powder was uniformly dispersed in anhydrous ethanol under ultrasound. Remove appropriate amount of sample solution and add it to the copper net. Then dried under infrared lamp irradiation.

3.3.3 Nitrogen Physical Isothermal Adsorption/Desorption

The SSA of the samples was calculated by means of the Brunauer-Emmett-Teller (BET) method and the pore size distribution was calculated using the Barrett-Joyner-Halenda (BJH) method from the desorption branch of the isotherms. The total pore volume was estimated from the amount of N_2 adsorbed at a relative pressure of P/P0 = 0.97.

Sample preparation: The sample powder was degassed at 120 ℃ for more than 12 hours before testing.

3.3.4 X-ray Diffraction

X-ray diffraction (XRD) data were determined on a Rigaku D/MAX-2500 X-ray diffractometer equipped with Cu-Kα radiation (λ = 1.541841 Å). It was used to test the crystalline or amorphous state in which the samples existed.

Sample preparation: Before testing, the sample is thoroughly ground into a uniform powder by an agate mortar and the particle size is controlled at about 40 microns. Then filled the sample powder into the microscope slide, after that flatten the sample plane, ready for measurement.

3.3.5 X-ray Photoelectron Spectroscopy

X-ray photoelectron spectroscopy (XPS) measurement was performed using the Thermo Scientific ESCALab250Xi system by applying an Al-Kα radiation. This characterization further reveals the element distribution and the surface elemental composition. The C1s spectrum (binding energy is 284.8 eV) of the carbon

contamination was used as charge correction. The sample were prepared by tablet pressing method.

3.4 Electrochemical Performance Evaluation

The electrochemical properties of all the samples were determined in a three/two electrode system in an electrochemical workstation (CHI760E). A Hg/HgO electrode and platinum wire were used as the reference electrode and the counter-electrode respectively in the three-electrode system and a 6M KOH solution was used as the electrolyte. Working electrodes were prepared by mixing samples, polytetrafluoroethylene and acetylene black with a mass ratio of 8:1:1. And the mixture was homogeneously mixed with ethanol and then dried at 100 ℃ overnight. The mass of the obtained mixture 9~13 mg was loaded on a nickel foam (1 cm^2). All the tests were carried out at room temperature. The electrochemical behaviors of all the samples were evaluated using Cyclic Voltammetry (CV), Galvanostatic Charge-Discharge (GCD) tests, Electrical Impedance Spectroscopy (EIS) and cycling stability techniques. In a two-electrode system, the same mass of samples is used as working electrode and counter-electrode respectively. The specific capacitance was calculated based on the total mass of the active materials. In the three-electrode system, the specific gravimetric capacitance (C, F g^{-1}) was calculated based on $C=I\,\Delta t/m\,\Delta V$, in which I (A), Δt (s), m (g) and ΔV (V) are current density, discharge time, mass of the active materials and the voltage change during the discharge process, respectively. For the two-electrode system, the specific gravimetric capacitance (C, F g^{-1}) was calculated based on $C=4\,I\,\Delta t/m\,\Delta V$,

in which I (A), Δt (s), m (g) and ΔV (V) are the same as those of the three-electrode system. According to $E = 0.5\ C\ (\Delta V)^2/4/3.6$, $P = 3600\ E/\Delta t$, the energy density (E, Wh kg^{-1}) and the power density (P, W kg^{-1}) were calculated, where I (A), Δt (s), ΔV (V) and m (g) are the current density, discharge time, voltage window and the mass of active materials, respectively.

CHAPTER 4

N-doped Porous Carbon Nanotubes Derived from Polypyrrole for High Performance Supercapacitors

(Notes: This work was published in Journal of Analytical and Applied Pyrolysis 152:104925, DOI: 10.1016/j.jaap.2020.104925.)

4.1 Introduction

Supercapacitors have various applications in electric vehicles, energy storage systems, and telecommunications (cellular phones, personal entertainment instruments). It can be considered potentially the most next-generation cleaner energy-storage devices.[1–4] The key components in supercapacitors are electrode materials, which determine the supercapacitors' ultimate electrochemical performance. Carbon materials are one of the potential electrode materials for supercapacitors.[5,6] Carbon nanotubes,[7,8] nanofibers,[9] nanospheres,[10,11] grapheme,[12] porous carbon,[13,14] and their hybrids[15] have also been widely used for supercapacitors. Although carbon materials have been studied for a long time, porous carbon nanotubes (PCNs), with their unique tubular morphology, high electrical conductivity, and low cost still dominate today's market of electrode materials for supercapacitors.[16] However, their low SSA, un-abundant pore structures, and inert surfaces limit the application of PCNs in supercapacitors. Mixed salt activation is a popular method for synthesizing high SSA and high-porosity carbon materials in recent years.[17,18] Here, novel nitrogen-doped porous carbon nanotubes (NCNs) were successfully synthesized by using polypyrrole (PPy) as carbon and nitrogen precursor, and mixed salts NaCl/$ZnCl_2$ as activator. The effects of the mixed

salts dosage, the difference between the mixed salts and the single salt (NaCl or $ZnCl_2$) and the carbonization temperature on the porosity were investigated. The obtained samples are characterized by high SSA (1,278 m^2g^{-1}), high nitrogen-doping (9.26 %), and plentiful pore structure (mesoporous size 3.1 nm), and they maintain a tubular morphology. In addition, the electrochemical performance of the obtained NCNs in supercapacitors were evaluated by using CV, GCD, EIS techniques, and so on. The facile and low-cost synthesis strategy shed light on the development of advanced porous carbon materials in supercapacitors.

4.2 Experiment

4.2.1 Preparation of PPy

PPy was synthesized by a modified oxidative template assembly route. Typically, 0.8 g of cetyltrimethylammonium bromide (CTAB) was dissolved in 240 ml of hydrochloric acid solution (1M HCl) in an ice bath (0-3 ℃) under continuous stirring to form a transparent solution. Then 1.2 g of ammonium persulfate [APS, $(NH_4)_2S_2O_8$,] was added to the above solution under magnetic stirring, and a white suspension solution was formed immediately. Afterward, 1.6 ml of pyrrole monomer was added dropwise to the white suspension under stirring, then the polymerization was carried out for 3 h while stirring. Finally, the precipitate was collected by filtration, washed with de-ionized water until the filtrate became colorless and the pH value was adjusted to neutral (pH=7.0). The black precipitate named PPy was obtained and then dried in freeze-drying equipment.

4.2.2 Preparation of NCNs-A

PPy and NaCl/$ZnCl_2$ (molar ratio 42:58) were mixed in various mass ratios by grinding in an agate mortar. Subsequently, the mixture were activated at different temperatures for 2h in a tubular furnace with N_2 gas flow to obtain NCNs-A. After naturally cooling down, the solid products were washed with sufficient 2M HCl aqueous solution and de-ionized water until the filtrate became clear, and then dried the solid at 100 ℃ overnight in an oven. A series of samples denoted as NCNs-A-1, NCNs-A, NCNs-A-2, NCNs-A-3 (the numbers 1, 2, and 3 represent the different mass ratios of PPy-to-mixed salts were 1:1, 1:5, and 1:10, respectively), NCNs-A was the mass ratio of 1:2 at 800 ℃ and NCNs-A-t, where t represented the different temperatures 600, 700, and 900 ℃. NCNs-A-N and NCNs-A-Z represented PPy only with NaCl and $ZnCl_2$ at a carbonization temperature of 800 ℃ respectively. In addition, for control purposes, the PPy without mixed salts and the carbonization temperature of 800 ℃ was denoted to NCNs.

4.3 Results and Discussion

4.3.1 Schematic Illustration

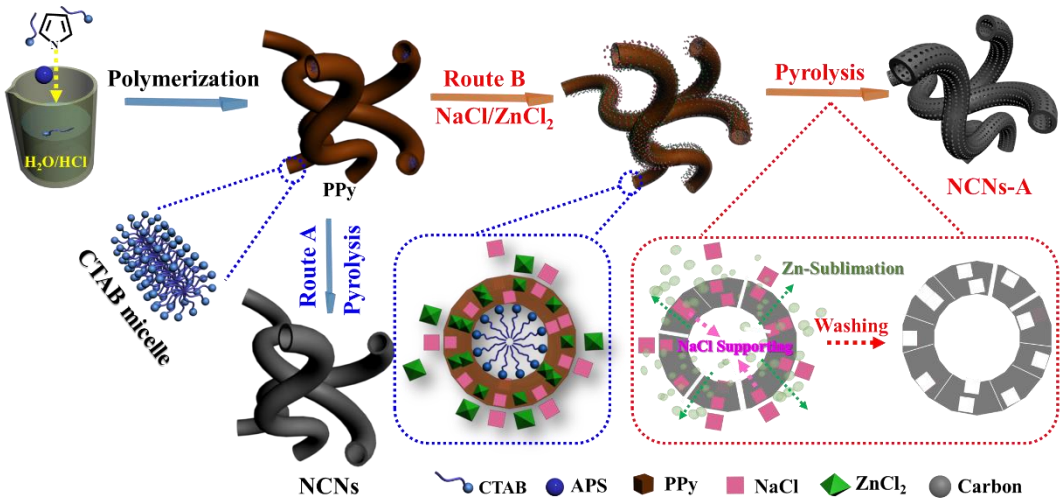

Fig. 4.1: Schematic illustration of the synthetic route of NCNs and NCNs-A

The synthesis procedure of NCNs-A is shown in Fig. 4.1 route B; simultaneously, the N-doped carbon nanotubes (NCNs) without an activation process was also prepared as a means of comparison. As carbon precursor, the tubular PPy was prepared by the polymerization of pyrrole monomer in HCl solution using CTAB as the structure-directing agent and APS as the initiator. The prepared NCNs derived from the direct thermal treatment of PPy (Fig. 4.1, route A) maintained the tubular morphology without obvious pores on the surface. However, to prepare the NCNs-A, the PPy was mixed with NaCl/$ZnCl_2$ to form PPy-NaCl-$ZnCl_2$ hybrid, as shown in route B of Fig. 4.1. During the pyrolysis procedure, $ZnCl_2$, as the activation agent, can sublimate at high temperature to create an abundant porous structure in the carbon framework.[19] Simultaneously, NaCl served as a supporting template, which can effectively guarantee

the tubular morphology.[20] After removing NaCl and residual zinc species, NCNs-A with a tubular morphology and an abundant porous structure can be obtained.

4.3.2 TEM Characterization

The morphology of NCNs and NCNs-A were analyzed by means of a transmission electron microscope (TEM).

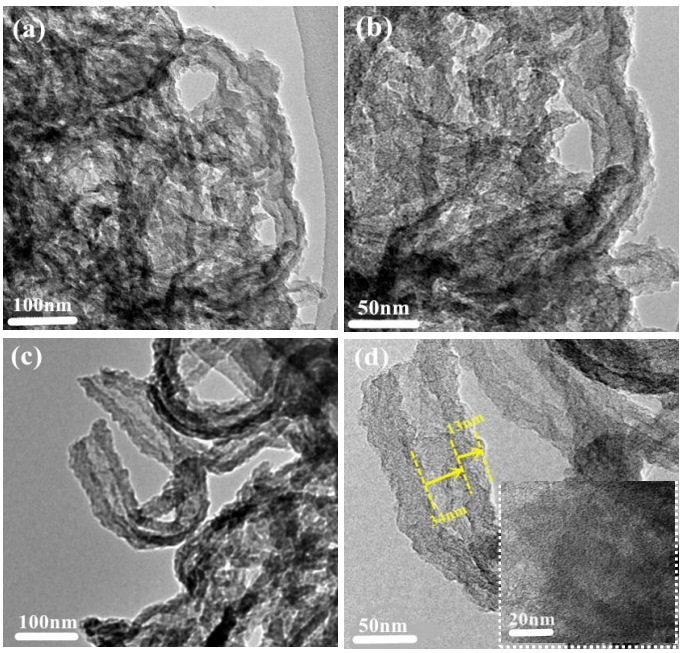

Fig. 4.2: (a) TEM image of NCNs and (b) the locally enlarged TEM image of NCNs; (c) TEM images of NCNs-A and (d) the locally enlarged TEM image of NCNs-A.

As shown in Fig. 4.2a and 4.2b, NCNs showed a curved, tube-like structure, with a rough surface. TEM images of NCNs clearly showed its rough surface and hollow tubular morphology with a diameter of 45 nm and a wall thickness of ca. 15 nm. After mixed salts activation, the NCNs-A still retained a tubular-like structure, which was similar to that of NCNs. However, compared to NCNs, the inner diameter of NCNs-A

is ca. 34 nm and the shell thickness was slightly thinner (13 nm) (Fig. 4.2c and 4.2d). The enlarged image (inset of Fig. 4.2d) clearly shows that NCNs-A has numerous pores consisting of amorphous carbon. The characteristics of porous structure and hollow tubular morphology of NCNs-A can provide a long, ionic pathway and increase the ion-accessible surface area, which enables NCNs-A as an electrode material to have excellent specific capacitance [21].

4.3.3 Surface Structure

N_2 isothermal adsorption-desorption measurements were carried out to confirm the pore structures of NCNs samples.

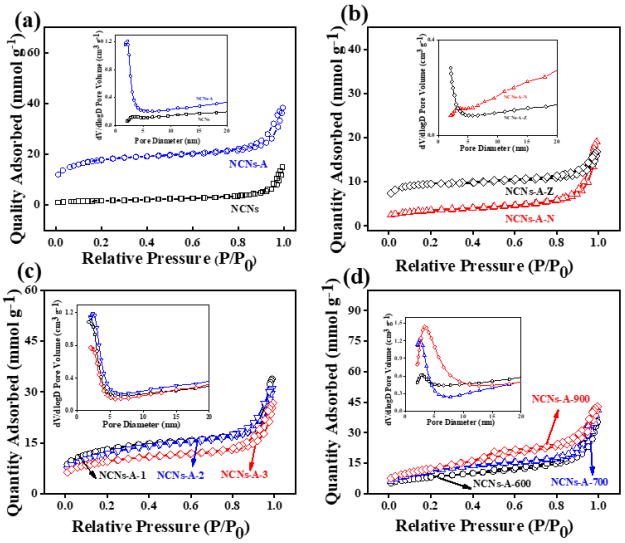

Fig. 4.3: N_2 adsorption-desorption isotherms and inset were the corresponding pore distribution curves of NCNs samples. (a) NCNs-A and NCNs; (b) NCNs-A-N, NCNs-A-Z; (c) NCNs-A-1, NCNs-A-2, NCNs-A-3; (d) NCNs-A-600, NCNs-A-700, NCNs-A-900.

As illustrated in Fig. 4.3a NCNs-A showed type IV adsorption-desorption isotherms with the apparent H3-type hysteresis loops in 0.4-0.9 (P/P_0), demonstrating the presence of a widespread mesoporous distribution.[22,23] However, the NCNs showed type IV adsorption-desorption isotherms and with a narrow hysteresis loop, indicating its poor porous structure. The pore-size distribution (inset of Fig. 4.3a) reveals the mesoporous size of 3.3 nm of NCNs-A, and the NCNs did not display an obvious mesoporous distribution. The specific surface area (SSA) and the total pore volume of the NCNs-A were calculated to be 1278 m^2g^{-1} and 1.49 cm^3g^{-1}, which is much higher than those of NCNs (136 m^2g^{-1} and 0.51 cm^3g^{-1}). The achieved high SSA, larger pore size and total

pore volume of NCNs-A were attributed to the sublimation of Zn and the high-energy chloride ions generated during the mixed salts activation process, which can etch the carbon skeleton to form a porous structure.[24,25]

To confirm the positive effect of mixed salts for the coordination of activation, the NaCl or $ZnCl_2$ was used separately to prepare NCNs-A-N and NCNs-A-Z. The porous properties of NCNs-A-N and NCNs-A-Z were tested by N_2 adsorption-desorption measurement, as presented in Fig. 4.3b, and the detailed textural parameters were provided in Table 4.1. From the Fig. 4.3b, NCNs-A-N showed a lower specific surface area than NCNs-A-Z, due to the invalid activation of individual NaCl in NCNs-A-N. $ZnCl_2$ is the common activation agent for preparing porous carbon materials.[26–28] Although the SSA has increased significantly for NCNs-A-Z, the activation effect of $ZnCl_2$ is unsatisfactory when compared to the mixed salts activation. There is no obviously mesoporous distribution in NCNs-A-N and NCNs-A-Z, as seen in the inset of Fig. 4.3b. Meaning that only $ZnCl_2$ existed could cause the collapse of the porous structure when no NaCl is added, which can serve as a supporting template to prevent pores from collapsing. In order to investigate the influence of the amount of mixed salts on the pore structure, NCNs-A samples with different composition (refers to the mass ratio of PPy to mixed salts) were also prepared. The N_2 adsorption-desorption isotherms of all samples (Fig. 4.3c) were similar to those of NCNs-A. In addition, the SSA first increases and then decreases with the increase in the amount of mixed salts, which confirms that the dosage of mixed salts is critical to the final samples and that excessive activation agent may collapse the pores.

The activation temperature can affect the sublimation rate of $ZnCl_2$ and the crystal state of NaCl, thus affecting the structural properties of activated products. Fig. 4.3d exhibited N_2 adsorption-desorption isotherms of the NCNs-A-600, NCNs-A-700, NCNs-A, and NCNs-A-900 in which 600, 700 and 900 refer to the activation temperature. Seen from the textural parameters in Table 4-1, the SSA was increased from 634 to 1,278 m^2g^{-1} and the total pore volume increased from 1.22 to 1.49 cm^3g^{-1} as the activation temperature increased from 600 to 800 ℃. This demonstrated that the mixed salts played a good role of porogen during the activation process. However, when the temperature reached 900 ℃, the pore structure may collapse, which leads to the SSA decreasing due to the melting of NaCl (melting point of 801 ℃) and it loses its supporting effect.[29] It followed that the activation effect of mixed salts was better than that of the individual salt, and the dosage of mixed salts, activation temperature also affects the final samples.

4.3.4 Surface Structure

The structure of the NCNs and NCNs-A were tested by X-ray diffraction (XRD).

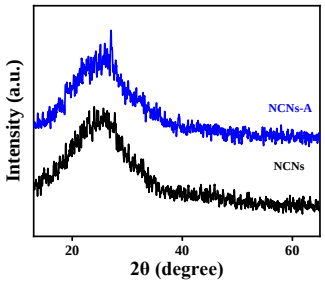

Fig. 4.4: X-ray diffraction (XRD) patterns of NCNs and NCNs-A

The XRD patterns of NCNs and NCNs-A were listed in Fig. 4.4. Both of them displayed

a broad diffraction peak, which is typical of carbon materials with rather disordered structures. This demonstrated that NCNs and NCNs-A were made of amorphous carbon[30] that is consistent with the TEM results in Fig. 4.2.

Detailed textural properties for all NCNs samples were listed in Table 4.1:

Table 4.1: Summary of textural properties for all samples

Samples	S_{BET} (m^2 g^{-1})	V_t (cm^3 g^{-1})[a]	S_{micro} (m^2 g^{-1})[b]	V_{micro} (cm^3 g^{-1})[c]	Pore size (nm)
NCNs	136	0.51	60	0.01	–
NCNs-A-1	903	1.14	347	0.09	2.1
NCNs-A	1278	1.49	450	0.15	3.3
NCNs-A-2	917	1.08	361	0.08	2.4
NCNs-A-3	717	0.93	293	0.09	2.1
NCNs-A-600	634	1.22	287	0.07	3.0
NCNs-A-700	880	1.42	286	0.03	2.7
NCNs-A-900	997	1.33	442	0.09	2.1
NCNs-A-N	256	0.66	123	0.14	–
NCNs-A-Z	661	0.58	312	0.05	2.1

[a]Total pore volume at P/P_0 = 0.97; [b]Micropore surface area determined by the t-plot method; [c]Micropore volume calculated by the t-plot method

4.3.5 Characterization of Surface Chemical Compositions

X-ray photoelectron spectroscopy (XPS) was used to analyze the chemical surface compositions of the NCNs-A.

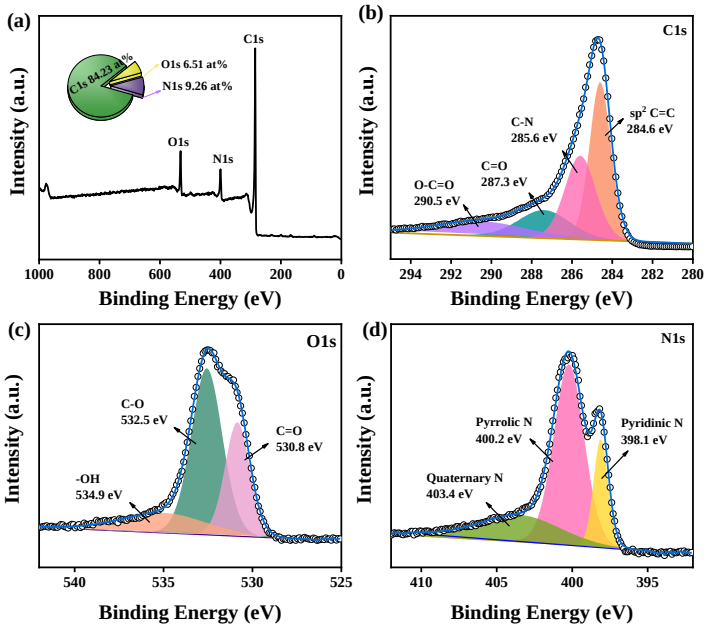

Fig. 4.5: (a) XPS spectrum of NCNs-A; (b) C1s spectrum; (c) O1s spectrum; (d) N1s spectrum

As presented in Fig. 4.5a, pronounced C1s, O1s and N1s peaks were observed in the survey spectrum. No absorption peaks of Zn, Na, or Cl were observed, indicating that all of impurities had been removed by hydrochloride acid. The XPS survey spectrum of the NCNs-A exhibited the C, N and O elements with content C (84.23 at%), N (9.26 at%), and O (6.51 at%). The high-resolution C1s spectrum in Fig. 4.5b was fitted by three individual component peaks located at 284.6, 285.7, and 288.6 eV, which corresponded to C-C, C-N, and C=O bonds, respectively. The deconvolution of the O1s regions in Fig. 4.5c of the spectra were assigned to three peaks, C=O (530.8 eV), C-O (532.5 eV) and O-H (534.9 eV). These oxygen species could be due to moisture, CO_2.[31] The N 1s spectra were fitted by three component peaks located at 398.1, 400.2 and 403.4 eV (Fig. 4.5d), respectively corresponding to pyridinic N, pyrrolic N and quaternary N.[32–34]

4.3.6 Electrochemical Performance of NCNs-A

The CV curves, GCD curves, and cycling performance of NCNs-A was evaluated by three-electrode configuration in 6M KOH solution.

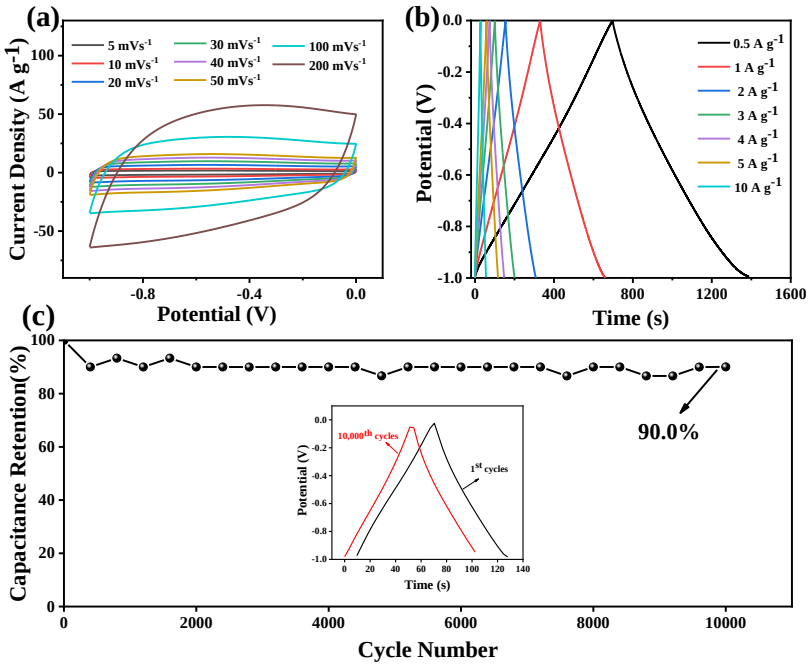

Fig. 4.6: Electrochemical characterization of NCNs-A tested by three electrode system in 6M KOH. (a) CV curves of NCNs-A at different scan rate; (b) GCD curves of NCNs-A at different current densities; (c) Cycling performance of NCNs-A electrode for charging and discharging at a current density of 5 A g^{-1}, insert is the first and the 10,000th cycles at 5 A g^{-1}

The prepared NCNs-A with both high specific surface area and appropriate pore distribution were expected to experience excellent capacitance performance, which was used as an active material in the working electrodes of supercapacitors. As shown in Fig. 4.6a, the CV curves of the NCNs-A exhibited a quasi-rectangular shape and maintain the quasi-rectangular shape even at a high scan rate (200 mV s^{-1}). This could be ascribed to the presence of a large number of mesopores in NCNs-A, which promote the charge transfer, indicating a favorable EDLC behavior with a good reversibility.[35]

The corresponding GCD curves were shown in Fig. 4.6b, all curves were nearly linear and show isosceles triangle shapes, even at the high density current of 10 A g^{-1}, revealing the rapid kinetics for charge-storage behavior and an excellent charge-transfer rate capability. In addition, NCNs-A were exhibited excellent electrochemical capacitance of 340 F g^{-1} at 1 A g^{-1}, indicating that NCNs-A had excellent capacitive performance as a supercapacitor electrode. A long cycling life is one of the important factors contributing to the performance of supercapacitors. The long-term cycle stability of NCNs-A was investigated by GCD measurement at 5 A g^{-1} after 10,000 charge/discharge cycles (Fig. 4.6c). It can be seen that the capacitance retention of NCNs-A was still maintained at 90.0 % through 10,000 charge/discharge cycles, which demonstrated an outstanding long-term cycling stability. These results demonstrated that the NCNs-A had the superior electrochemical performance.

The electrochemical performance of all NCNs samples were investigated.

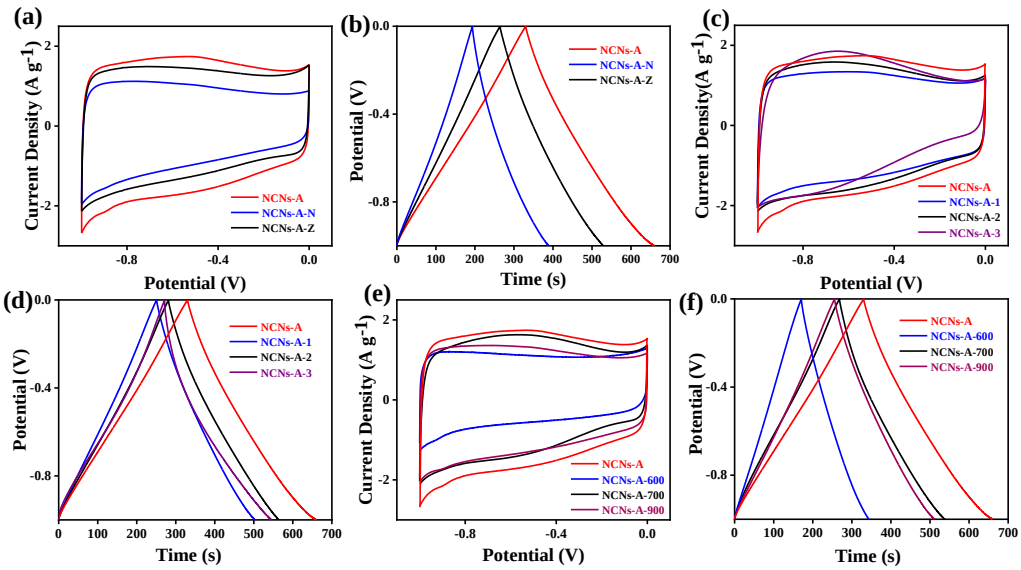

Fig. 4.7: Electrochemical characterization of NCNs-A, NCNs-A-N, NCNs-A-Z, NCNs-A-1, NCNs-A-2, NCNs-A-3, NCNs-A-600, NCNs-A-700, NCNs-A-900 tested by three electrode system in 6M KOH: (a, c, e) CV curves at scan rate of 5 mV s^{-1}; (b, d, f) GCD curves at current

densities of 1 A g^{-1} of NCNs-A-600, NCNs-A, NCNs-A-700, NCNs-A-900, NCNs-A-1, NCNs-A-2, NCNs-A-3, NCNs-A-N, NCNs-A-Z, NCNs

Other proportions and different carbonization temperatures of samples were also tested for electrochemical performance in supercapacitors. From Fig. 4.7(a, c, e), compared to other samples, the area under the CV curve of NCNs-A was the largest of all the samples, demonstrating an enhanced specific capacitance again. Fig. 4.7(b, d, f) show the GCD curves and the NCNs-A were exhibited excellent electrochemical capacitance that was superior to other samples (for the data see Table 4-2).

The electrochemical properties of NCNs samples are summarized in the following table:

Table 4.2: Electrochemical performance of samples

Samples	Capacitance/(Fg^{-1})	SCR/(%)[a]
NCNs	151	79.2
NCNs-A-1	251	82.0
NCNs-A	340	83.0
NCNs-A-2	290	81.2
NCNs-A-3	283	50.5
NCNs-A-600	179	81.5
NCNs-A-700	276	76.5
NCNs-A-900	264	82.0
NCNs-A-N	201	76.9
NCNs-A-Z	266	78.0

[a] Specific capacitance retention.

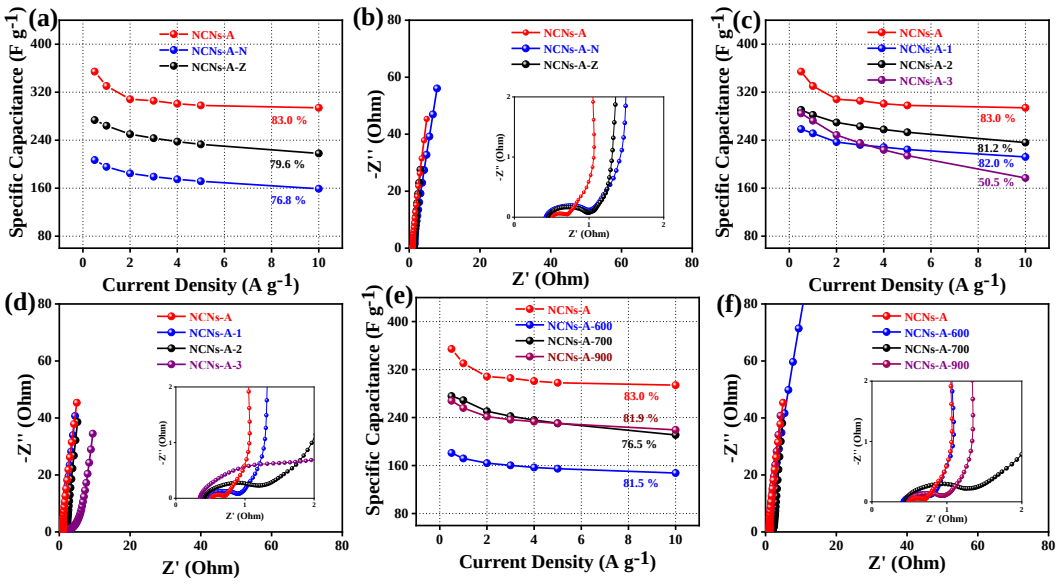

Fig. 4.8: Specific capacitance and Nyquist plots of NCNs-A, NCNs-A-N, NCNs-A-Z, NCNs-A-1, NCNs-A-2, NCNs-A-3, NCNs-A-600, NCNs-A-700, NCNs-A-900: (a, c, e) Specific capacitances at different current densities from 0.5 A g^{-1} to 10 A g^{-1}; (b, d, f) the Nyquist plots with fitting curves and corresponding high-frequency ranges (inset) of samples.

Rate capability is a vital indicator for evaluating electrode materials in supercapacitors. The contrast of the specific capacitance at the range of 0.5 to 10 A g^{-1} were shown in Fig. 4.8(a, c, e). It can be seen that NCNs-A had the higher value of 83.0 % and NCNs is 79.2 %, showed a superior rate capability. This may be attributed to large SSA and an abundant porous structure, providing more ion adsorption space, and facilitates ion diffusion.[36] The prefabricated NCNs and NCNs-A were further evaluated by using EIS to study the ion diffusion and the charge transfer inside the electrodes. According to the Nyquist plots shown in Fig. 4.8b, d, and f, all of the samples showed almost similar outlines. All of them with a semicircle in high-frequency regions (related to the power performance and internal resistance of the samples) and an approximately vertical line in the low frequency, indicating an ideal capacitive behavior of EDLC.[37] It was noted that NCNs-A had the minimum radius, and in the low-frequency region the line is more vertical, which implies good capacitive performance. It is indicated that the NCNs-A displayed excellent ion diffusion and charge transportation behavior compared to NCNs. All the results proved that the optimal synthesis condition is the mass ratio in PPy to molten salts of 2 and a carbonization temperature at 800 ℃. To investigate the electrochemical performance of NCNs-A further in practical application, symmetric supercapacitors based on NCNs-A were assembled in a two-electrode system which used a 6M KOH solution as electrolyte.

The capacitive performance of NCNs-A was further inspected in two-electrode system.

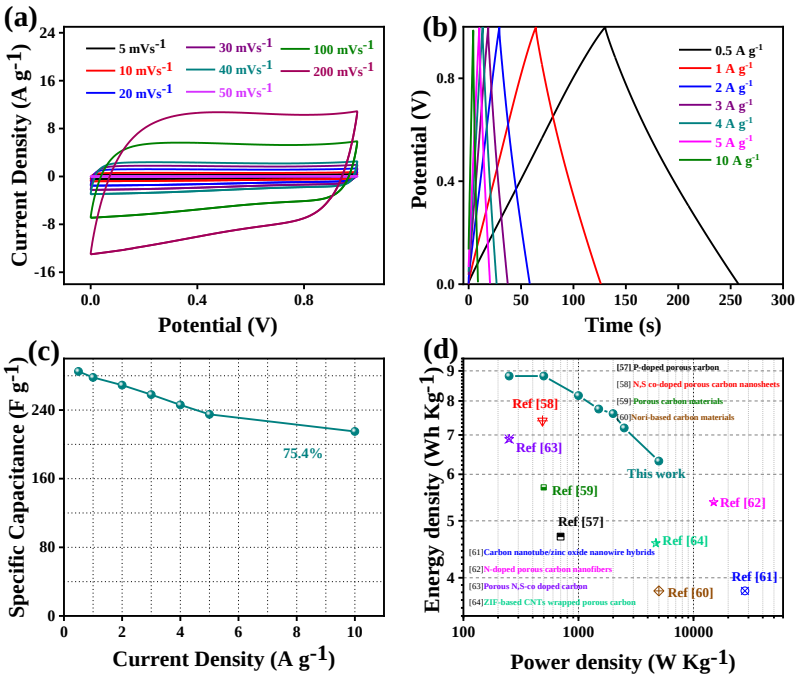

Fig. 4.9: (a, b) CV curves and GCD curves of NCNs-A at 5-200 mV s^{-1} and electric density of 0.5-10 A g^{-1}; (c) Specific capacitance of the NCNs-A at a current density of 5 A g^{-1}; (d) Ragone plots of NCNs-A in a two-electrode system

Fig. 4.9a displayed a quasi-rectangular shape of CV curves of NCNs-A even at the high scan rate of 200 mV s^{-1}, which proved to be highly reversible; GCD curves from 0.5 to 10 A g^{-1} were showed a triangular characteristic in Fig. 4.9b. The specific capacitance was calculated to be 285 F g^{-1} at a current density of 1 A g^{-1} and 215 F g^{-1} at a current density of 10 A g^{-1}, respectively (Fig. 4.9c). The NCNs-A achieved a maximum energy density of 8.82 Wh kg^{-1} at a power density of 0.25 KW kg^{-1} in 6M KOH electrolyte, and still retained an energy density of 6.32 Wh kg^{-1} at a power density of 5 KW kg^{-1} as shown in Fig. 4.9d. Notably, at corresponding energy density, NCNs-A had relatively higher power output capability compared to other carbon materials, include carbon

nanofibers and carbon nanosheets,[38-45] exhibiting high performance and demonstrating further the superior performances of NCNs-A as an electrode.

4.4 Conlusion

In this section, NCNs-A with a high specific surface area (1278 m^2 g^{-1}), high nitrogen content (9.26 %) and plentiful porous structure were successfully prepared by mixed salts activation. The physical and chemical characterization of the obtained NCNs-A indicated that the pore structures, specific surface area, and electrochemical performance of all the samples are affected by the molar ratio of PPy to NaCl/$ZnCl_2$, and the carbonization temperature. In the case of the obtained NCNs-A with the tube-like morphology, the inner diameter of the NCNs-A becomes larger and the wall thickness of the tube becomes thinner than that of NCNs. Electrochemical characterization demonstrated that NCNs-A has a maximum capacitance of 340 F g^{-1} at 1 A g^{-1}, a long-term stability of 90.0 % after 10,000 cycles, and outstanding electrochemical performance than other carbon materials. We look forward to these simple, controllable synthetic carbon materials that can have a wide range of applications in the fields of adsorption, catalysis and energy storage.

References

[1] Yu X Y, and Lou X W. Mixed metal sulfides for electrochemical energy storage and conversion. Advanced Energy Materials. 2018, 8(3): 1701592.

[2] Nai J, and Lou X W. Hollow structures based on Prussian blue and its analogs for electrochemical energy storage and conversion. Advanced Materials. 2019, 31(38): 1706825.

[3] Hou X Y, Peng T, Yu Q H, Luo R J, Liu X M, Zhang Y G, Wang Y G, Guo Y, Kim J-K, and Luo Y S. Facile synthesis of Holothurian-like γ-MnS/carbon nanotube nanocomposites for flexible all-solid-state supercapacitors. Chem. Nano Mat. 2017, 3(8): 551-559.

[4] Wang N, Wang Y J, Cui S Z, Hou H W, Mi L W, and Chen W H. A hollow tube-on-tube architecture of carbon-tube-supported nickel cobalt sulfide nanotubes for advanced supercapacitors. Chem. Nano Mat. 2017, 3(4): 269-276.

[5] Santucci A, Sorniotti A, and Lekakou C. Power split strategies for hybrid energy storage systems for vehicular applications. Journal of Power Sources. 2014, 258: 395-407.

[6] Kouchachvili L, Ya ïci W, and Entchev E. Hybrid battery/supercapacitor energy storage system for the electric vehicles. Journal of Power Sources. 2018, 374: 237-248.

[7] Zhu S M, Dong X F, Huang H, and Qi M. Rich nitrogen-doped carbon on carbon nanotubes for high-performance sodium-ion supercapacitors. Journal of Power Sources, 2020, 459:228104.

[8] Ha P T, Moon H, Kim B H, Ng H Y, and Chang I S. Determination of charge transfer resistance and capacitance of microbial fuel cell through a transient response analysis of cell voltage. Biosensors and Bioelectronics. 2010, 25(7): 1629-1634.

[9] Ma C, Wu L Q, Dirican M, Cheng H, Li J J, Song Y, Shi J L, and Zhang X W. Carbon black-based porous sub-micron carbon fibers for flexible supercapacitors. Applied Surface Science, 2021, 537:147914.

[10] Javaid A. Activated carbon fiber for energy storage. 2017, 281-303.

[11] Yu J L, Lu W B, Pei S P, Gong K, Wang L Y, Meng L H, Huang Y D, Smith J P, Booksh K S, Li Q W, Byun J-H, Oh Y, Yan Y, and Chou T-W. Omnidirectionally stretchable high-performance supercapacitor based on isotropic buckled carbon nanotube films. ACS Nano. 2016, 10(5): 5204-5211.

[12] Wan L, Shamsaei E, Easton C D, Yu D B, Liang Y, Chen X F, Abbasi Z, Akbari A, Zhang X W, and Wang H T. ZIF-8 derived nitrogen-doped porous carbon/carbon nanotube composite for high-performance supercapacitor. Carbon. 2017, 121: 330-336.

[13] Zhang L J, Jiang Y Z, Wang L W, Zhang C, and Liu S X. Hierarchical porous carbon nanofibers as binder-free electrode for high-performance supercapacitor. Electrochimica Acta. 2016, 196: 189-196.

[14] Bin D S, Chi Z X, Li Y, Zhang K, Yang X Z, Sun Y G, Piao J Y, Cao A M, and Wan L J. Controlling the compositional chemistry in single nanoparticles for functional hollow carbon nanospheres. Journal of the American Chemical Society. 2017, 139(38): 13492-13498.

[15] Du J, Zhang Y, Wu H X, Hou S L, and Chen A B. N-doped hollow mesoporous carbon spheres by improved dissolution-capture for supercapacitor. Carbon. 2020, 156: 523-528.

[16] Zhou J S, Hou L, Lian J, Cheng W B, Wang D, Gou H Y, and Gao F M. Nitrogen-doped highly dense but porous carbon microspheres with ultrahigh volumetric capacitance and rate capability for supercapacitors. Journal of Materials Chemistry. 2019, 7(2): 476-485.

[17] Fechler N, Fellinger T P, and Antonietti M. “Salt templating”: A simple and sustainable pathway toward highly porous functional carbons from ionic liquids. Advanced Materials. 2013, 25(1): 75-79.

[18] Han X Y, Zhang Y F, Wan J, Xu W N, Li J E, Hu C G, Liu G L, and Cheng X L. An activated carbon cloth anode obtained with a fast molten salt method for high-performance supercapacitors. Journal of Alloys and Compounds, 2020, 838:155695.

[19] Hao J N, Huang Y J, He C, Xu W J, Yuan L B, Shu D, Song X N, and Meng T. Bio-templated fabrication of three-dimensional network activated carbons derived from mycelium pellets for supercapacitor applications. Scientific Reports. 2018, 8(1): 562-562.

[20] Zhu S, Li J J, He C N, Zhao N Q, Liu E Z, Shi C S, and Zhang M. Soluble salt self-assembly-assisted synthesis of three-dimensional hierarchical porous carbon networks for supercapacitors. Journal of Materials Chemistry. 2015, 3(44): 22266-22273.

[21] Ranu R, Chauhan Y, Ratan A, Yadav S, and Tomar S K. Multifunctional biogenically synthesized porous multi-walled carbon nanotubes dispersed polymer electrolyte-based supercapacitor. Applied Physics A. 2020, 126(3): 1-9.

[22] Zheng X J, Cao X C, Li X W, Tian J H, Jin C, and Yang R Z. Biomass lysine-derived nitrogen-doped carbon hollow cubes via a NaCl crystal template: An efficient bifunctional electrocatalyst for oxygen reduction and evolution reactions. Nanoscale. 2017, 9(3): 1059-1067.

[23] Liu X F, and Antonietti M. Molten salt activation for synthesis of porous carbon nanostructures and carbon sheets. Carbon. 2014, 69: 460-466.

[24] Ma Z S, Zhang H Y, Yang Z Z, Zhang Y F, Yu B, and Liu Z M. Highly mesoporous carbons derived from biomass feedstocks templated with eutectic salt $ZnCl_2$/KCl. Journal of Materials Chemistry A. 2014, 2(45):19324-19329.

[25] Huang L, Hu Z M, Jin H R, Wu J B, Liu K S, Xu Z H, Wan J, Zhou H, Duan J J, Hu B, and Zhou J. Salt-assisted syndissertation of 2D materials. Advanced Functional Materials. 2020, 1908486.

[26] Wang H L, Zhang L B, Deng T S, Ruan H, Hou X L, Cort J R, and Yang B. $ZnCl_2$-induced catalytic conversion of softwood lignin to aromatics and hydrocarbons. Green Chemistry. 2016, 18(9): 2802-2810.

[27] Zhang S P, Zhu S G, Zhang H L, Liu X Z, and Xiong Y Q. Synthesis and characterization of rice husk-based magnetic porous carbon by pyrolysis of pretreated rice husk with $FeCl_3$ and $ZnCl_2$. Journal of Analytical and Applied Pyrolysis. 2020.

[28] Li B Q, Cheng Y F, Dong L P, Wang Y M, Chen J C, Huang C F, Wei D P, Feng Y J, Jia D C, and Zhou Y. Nitrogen doped and hierarchically porous carbons derived from chitosan hydrogel via rapid microwave carbonization for high-performance supercapacitors. Carbon. 2017, 122: 592-603.

[29] Tang D H, Hu S, Dai F, Yi R, Gordin M L, Chen S R, Song J X, and Wang D H. Self-templated synthesis of mesoporous carbon from carbon tetrachloride precursor for supercapacitor electrodes. Acs Appl. Mater. Interfaces. 2016: 6779-6783.

[30] Tzeng S-S, and Chr Y-G. Evolution of microstructure and properties of phenolic resin-based carbon/carbon composites during pyrolysis. Materials Chemistry and Physics. 2002, 73(2-3): 162-169.

[31] Collins P G, Bradley K, Ishigami M, and Zettl A. Extreme oxygen sensitivity of electronic properties of carbon nanotubes. Science. 2000, 287(5459): 1801-1804.

[32] Desimoni E, Casella G I, and Salvi A M. XPS/XAES study of carbon fibers during thermal annealing under UHV conditions. Carbon. 1992, 30(4): 521-526.

[33] Biniak S, Szymański G, Siedlewski J, and Świątkowskib A. The characterization of activated carbon with oxygen and nitrogen surface groups. Carbon. 1997, 35(12): 1799-1810.

[34] Zhou H H, Han G Y, Xiao Y M, Chang Y Z, and Zhai H J. Facile preparation of polypyrrole/graphene oxide nanocomposites with large areal capacitance using electrochemical codeposition for supercapacitors. Power Sources. 2014, 263: 259-267.

[35] Lahe äär A, Przygocki P, Abbas Q, and Bé guin F. Appropriate methods for evaluating the efficiency and capacitive behavior of different types of supercapacitors. Electrochemistry Communications. 2015, 60: 21-25.

[36] Liu T Y, Zhang F, Song Y, and Li Y. Revitalizing carbon supercapacitor electrodes with hierarchical porous structures. Journal of Materials Chemistry. 2017, 5(34): 17705-17733.

[37] Zhao J, Li Z J, Yuan X C, Yang Z, Zhang M, Meng A, and Li Q D. A high-energy density asymmetric supercapacitor based on Fe_2O_3 nanoneedle arrays and $NiCo_2O_4$/$Ni(OH)_2$ hybrid nanosheet arrays grown on SiC nanowire networks as free-standing advanced electrodes. Advanced Energy Materials. 2018, 8(12): 1702787.

[38] Yi J N, Qing Y, Wu C T, Zeng Y X, Wu Y Q, Lu X H, and Tong Y X. Lignocellulose-derived porous phosphorus-doped carbon as advanced electrode for supercapacitors. Journal of Power Sources. 2017, 351:130-137.

[39] Miao L, Zhu D Z, Liu M X, Duan H, Wang Z W, Lv Y K, Xiong W, Zhu Q J, Li L C, Chai X L, and Gan L H. Cooking carbon with protic salt: Nitrogen and sulfur self-doped porous carbon nanosheets for supercapacitors. Chemical Engineering Journal. 2018, 347: 233-242.

[40] Sun Q Y, Jiang T Y, Zhao G Z, and Shi J Y. Porous carbon material based on biomass prepared by MgO template method and $ZnCl_2$ activation method as electrode for high performance supercapacitor. International Journal of Electrochemical Science. 2019, 14: 1-14.

[41] Wang C S, and Liu T Z. Nori-based N, O, S, Cl co-doped carbon materials by chemical activation of $ZnCl_2$ for supercapacitor. Journal of Alloys and Compounds. 2017, 696: 42-50.

[42] Alasadi A S, Henley L A, Wasala M, Muchharla1 B, Perea-Lopez N, Carozo V, Lin Z, Terrones M, Mondal K, Kordas K, and Talapatra S. Aligned carbon nanotube/zinc oxide nanowire hybrids as high-performance electrodes for supercapacitor applications. Journal of Applied Physics. 2017, 121(12): 124303.

[43] Chen L F, Zhang X D, Liang H W, Kong M G, Guan Q F, Chen P, Wu Z Y, and Yu S H. Synthesis of nitrogen-doped porous carbon nanofibers as an efficient electrode material for supercapacitors. ACS Nano. 2012, 6(8):7092-7102.

[44] Wu D L, Cheng J Y, Wang T, Liu P G, Yang L, and Jia D Z. A novel porous N- and S-self-doped carbon derived from Chinese rice wine lees as high-performance electrode materials in a supercapacitor. ACS Sustainable Chem. Eng. 2019, 7(14): 12138-12147.

[45] Yang L, Feng Y, Yu D B, Qiu J H, Zhang X F, Dong D H, and Yao J F. Design of ZIF-based CNTs wrapped porous carbon with hierarchical pores as electrode materials for supercapacitors. Journal of Physics and Chemistry of Solids. 2018, 125: 57-63.

CHAPTER 5

Salt Template-assisted Monomer Deposition Synthesis N-doped Porous Carbon for Supercapacitors

(Note: This research is expected to appear in the journal of Colloids and Surfaces B: Biointerfaces)

5.1 Introduction

As an ESD with great potential, supercapacitors, have received much attention in recent years. As is well known, for supercapacitors, ideal electrode materials with high electrochemical performance should have the following characteristics:

(1) A hierarchical, porous structure and high SSA in which the pore size distribution is well balanced;

(2) With higher conductivity and a low charge transfer resistance for achieving high power density and rate capability;

(3) Electrode materials must display excellent electrolyte compatibility and corrosion resistance for improving the cycling stability.[1]

Two dimension (2D) carbon materials of a large lateral size have a unique layered structure, an abundant and accessible catalytically active site, and unusual physical, chemical, and electronic properties, which makes them more attractive electrode candidates for supercapacitors.[2] To date, numerous 2D carbon materials, including transition metal dichalcogenides,[3] layered double hydroxides,[4] metal carbides (MXenes),[5] and porous carbon nanosheets (PCNs),[6] have been successfully

synthesized and applied in supercapacitors. Many ways of synthesizing 2D carbon materials have been reported, including: chemical vapor deposition (CVD),[7] solvothermal synthesis,[8] chemical or physical exfoliation,[9] and self-assembly.[10] But there are some shortcomings in these methods, such as: A limited carbon source (CVD; only gaseous hydrocarbons and volatile organic molecules can be used as carbon sources); for solvothermal synthesis, the higher operating temperature; the mechanism by which the nucleation occurs is not clear; and the temperature, pressure, and pH affect the resulting carbon morphologies and structure, for which there is still no clear solution; and some routes are time-consuming to process. Since NaCl are stable, low cost, and easy to be removed by water washing, it has been extensively explored as an important salt-template to fabricate porous carbon nanomaterials.[11] Differently from other template methods, the NaCl "salt template" synthesis process does not involve the use of toxic or harmful reagents such as HF or NaOH, which is used to remove templates.[12] Therefore, it is an environmentally friendly synthesis route. In this section, we proceed to investigate a promising electrode material for supercapacitors via a facile, effective and scalable salt template-assisted monomer deposition strategy. In this deposition strategy we adopted 3-aminophenol (3-A) as the carbon and nitrogen precursor, NaCl as the in-situ salt template, and $Co(NO_3)_2\ 6H_2O$ as the catalyst to synthesize nitrogen-doped carbon nanosheets (NPC). The dosage of NaCl required to influence the final properties of the samples was investigated. Due to the large SSA and a rich pore structure of NPC-20, when used as the electrode material for supercapacitors, it exhibited excellent electrochemical performance. The simple, low-cost,

environmentally friendly and scalable route to designing electrodes with a high-rate performance and also a long cycling stability performance in supercapacitors has provided some new avenues to pursue.

5.2 Experiment

5.2.1 Preparation of NPC

To prepare NPC, 1.0 g 3-A, 0.5 g $Co(NO_3)_2$ $6H_2O$, and 20 g NaCl were mixed by grinding them in anagate mortar. Then the mixture was dissolved in a certain amount of de-ionized water. The resulting solution was then freeze-dried in a vacuum and ground by agate mortar again to obtain a uniform powder. Finally, the composite powder was carbonized at 700 °C in N_2. The series of the NPC were obtained after etching the salt template and the metal impurities. For the purposes of comparison, the NPC-0, NPC-10, and the NPC-40 were obtained with different masses of NaCl: 0 g, 10 g, 40 g.

5.3 Results and Discussion

5.3.1 Synthesis Route of NPC

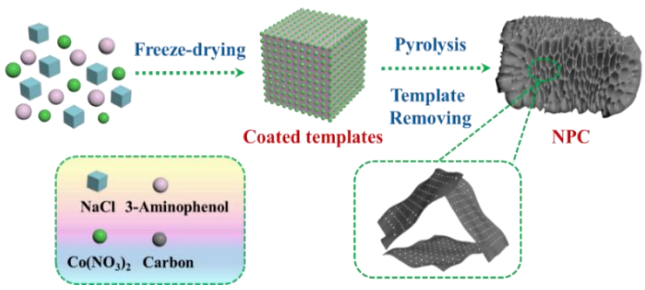

Fig. 5.1: Synthesis pathway for the fabrication of NPC

The synthetic strategy is illustrated in Fig. 5.1. In the beginning, 3-A as carbon and nitrogen precursor, $Co(NO_3)_2$ $6H_2O$ as the catalyst, NaCl as the salt template, are thoroughly mixed and dissolved. Subsequently, in the freeze-drying process, the mixture self-assemble. During pyrolysis, 3-A decomposes at a high carbonization temperature and self-deposits on the salt template; it then transforms into carbon on the metal catalyst, resulting in an efficient preparation of NPC.

In this process, the NaCl salt template played an important role in controlling the morphology and pore structure of the sample. It can remain relatively stable after calcination, a facile self-template was generated during the reaction process which can easily be removed, which can facilitates the formation of a porous morphology. The effect of the different dosages of NaCl on the final properties of the NPC were investigated.

5.3.2 SEM and TEM of NPC Samples

The morphology of NPC was characterized by SEM and TEM.

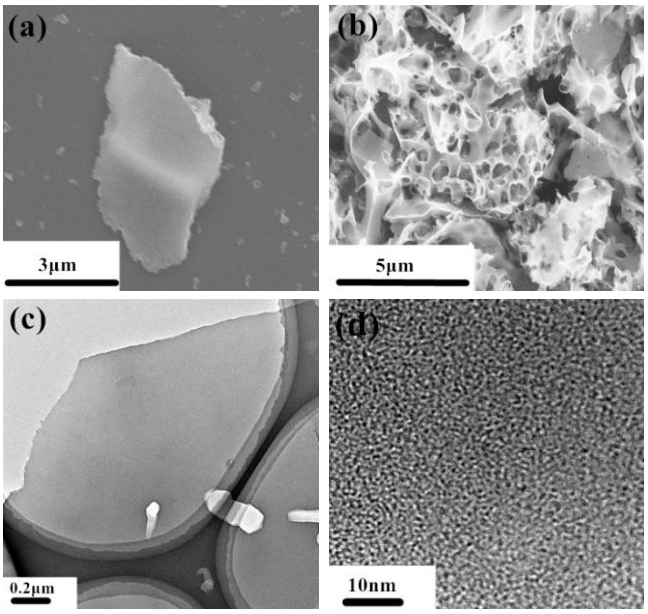

Fig. 5.2: (a) SEM images of NPC-0; (b, c, d) SEM and TEM images of NPC-20.

The different structure and characteristics of NPC-0 and NPC-20 are shown in Fig. 5.2(a-d). Compared to Fig. 5.2a and 5.2b, it can be concluded that NPC-0 exhibited a block-like shape and NPC-20 exhibited macropore structure, which demonstrated the template-like role of NaCl.[13] The TEM image (Fig. 5.2c and d) further confirmed the flake-like structure and uniform porous structure in large scale. These porous structure can provide a large surface area for excellent specific capacitance in supercapacitors.[14]

5.3.3 XPS Characterization of NPC-20

The chemical composition of the prepared samples is revealed using X-ray photoelectron spectroscopy (XPS).

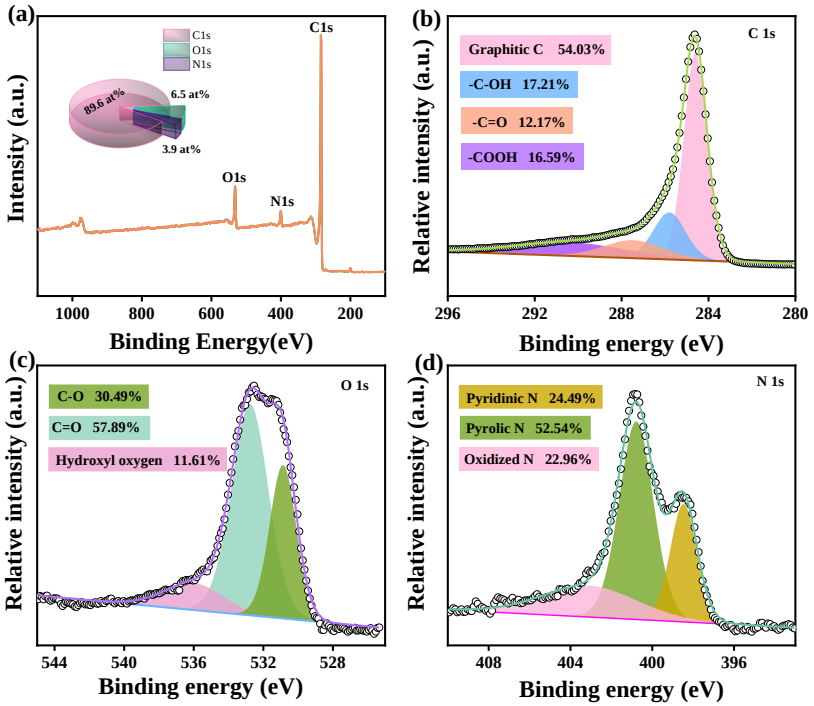

Fig. 5.3: (a) XPS survey spectrum of NPC-20; (b) C1s spectrum; (c) O1s spectrum; (d) N1s spectrum

The XPS results in Fig. 5.3a indicated the C, O, N elements that existed in NPC-20, the content being C (89.64 at%), O (6.50 at%), and N (3.86 at%), respectively. The benefits of heteroatom doped from the presence of nitrogen in 3-A, which can enhance the wettability of the NPC-20. This leads to a significant increase in the active surface area accessible to the electrolyte and increases the specific capacitance performance when used as electrode material in supercapacitors.[15,16] The XPS reveals no Co or Na species, which indicates that the metal ions are all completely removed. The high-resolution C1s

spectrum showed four peaks (Fig. 5.3b), these corresponding to graphitic C (284.6 eV, 54.03 %), C-OH (285.8 eV, 17.21 %), C=O (287.4 eV, 12.17 %), and COOH (290.51 eV, 16.59 %), respectively.[17] The O1s could be divided into three peaks (Fig. 5.3c), which can be assigned to C-O (530.9 eV, 30.49 %), C=O (532.8 eV, 57.89 %), and hydroxyl oxygen (536.0 eV, 11.61 %), respectively.[18] Meanwhile, the N1s spectrum of NPC possessed three peaks at 398.5, 400.8 and 403.1 eV; these represent pyridinic N (24.49 %), pyrolic N (52.54 %), and oxidized N (22.96 %) species, respectively (shown in Fig. 5.3d).[19]

5.3.4 Electrochemical Performance of NPC Samples

To evaluate the electrochemical performance of the NPC samples as supercapacitor electrodes, CV, GCD and EIS measurements were tested in a three-electrode system in 6M KOH electrolyte.

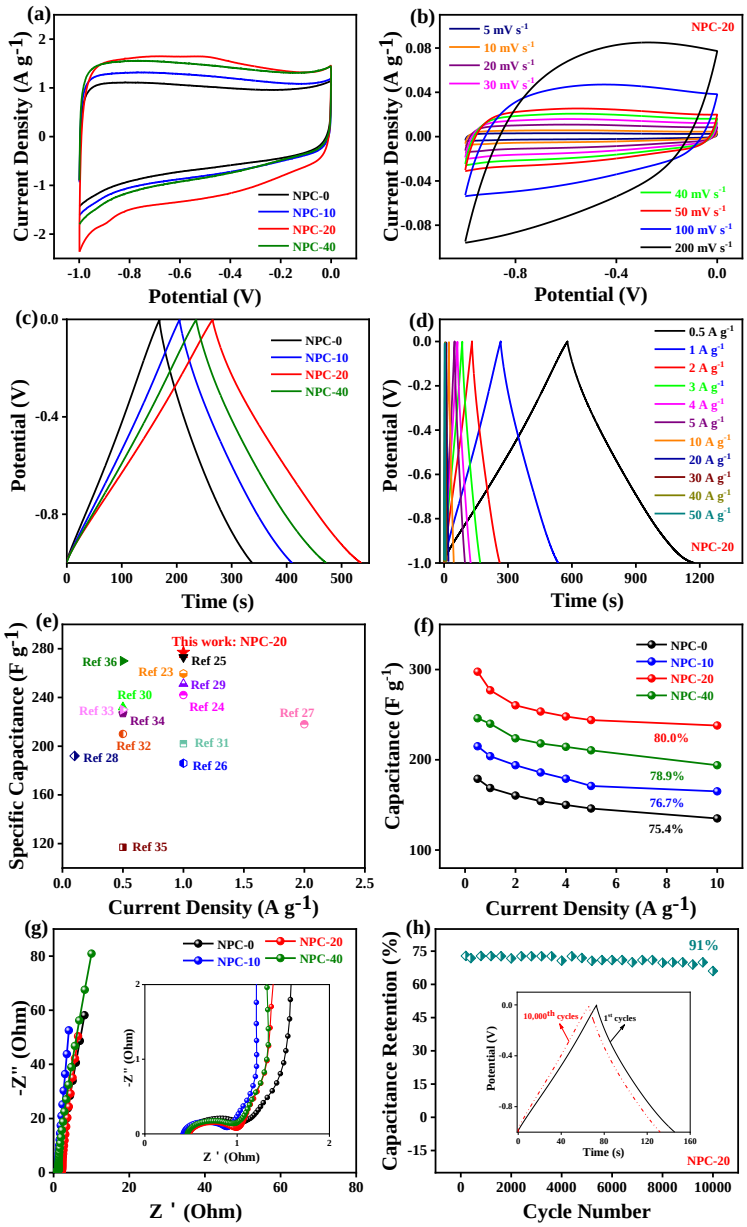

Fig. 5.4: Electrochemical performance of NPC samples in a three-electrode system in 6M KOH electrolyte. (a) CV curves of NPC samples at a scan rate of 5 mV s^{-1}; (b) CV curves of NPC-20 at different scan rate from 5 to 200 mV s^{-1}; (c) GCD curves of NPC samples at a current density of 1

A g^{-1}; (d) GCD curves of NPC-20 at different current densities, from 0.5 A g^{-1} to 50 A g^{-1}; (e) Specific capacitance comparison of NPC-20 with other carbon materials; (f) Rate performance of NPC samples at different current densities, from 0.5 A g^{-1} to 10 A g^{-1}; (g) Nyquist plots of NPC samples (inset magnifies the data in the high-frequency range); (h) Cycling stability of NPC-20 electrode for charging and discharging at 5 A g^{-1} (inset picture shows the first and the 10,000 th cycles)

Fig. 5.4a showed the CV plots of the NPC samples obtained by a scan rate of 5 mV s^{-1}. All the CV curves of the NPC samples were quasi-rectangular, representing an ideal double-layer capacitor behavior and a reversible adsorption or desorption for the ions process.[20,21] In addition, NPC-20 displayed a much larger CV curve-enclosed area than others, indicating its best capacitance characteristic. Fig. 5.4b showed the CV curves of NPC-20 at different scan rates. It could be concluded that all the curves have rectangular characteristics and maintained this rectangular-like shape at 200 mV s^{-1}, manifesting more ideal capacitive behavior. The GCD curves in Fig. 5.4c indicated that the NPC samples have good symmetry and nearly linear discharge slopes at the current density of 1 A g^{-1}. This indicated a typical feature of electrical double-layer capacitors.[22] Calculated from the GCD curves, NPC-20 apparently showed the longest charge–discharge time, and the specific capacitance is 277 F g^{-1} at 1 A g^{-1} obviously higher than that for NPC-0 (170 F g^{-1}), NPC-10 (204 F g^{-1}), or NPC-40 (240 F g^{-1}). The GCD curves of NPC-20 at different current densities were illustrated in Fig. 5.4d. All of them revealed triangular symmetrical distributions, confirming the typical EDLC behavior. Fig. 5.4e showed the specific capacitance comparison of NPC-20 with other carbon

materials: NPC-20 had a significantly higher capacitance value than other carbon materials,[23–36] which indicates the excellent supercapacitor performance of NPC-20. Based on the GCD results, the values of specific capacitance were recorded at current densities of 0.5 A g^{-1}-10 A g^{-1} (in Fig. 5.4f); and the outstanding rate capability of NPC-20 can be observed as 80.0 %. In Fig. 5.4g, the Nyquist plots showed a semi-circle which is related to the charge transfer resistance between the electrode and the electrolyte interface at high frequency.[37] The slope of the curves at low frequency represents the speed of ion transfer.[38] Compared to other samples, NPC-20 had the smallest semi-circle, which means that it has the lowest charge transfer resistance of 0.50 Ω (NPC-0: 0.60 Ω, NPC-10: 0.52 Ω, and NPC-40: 0.55 Ω). As shown in Fig. 5.4h, NPC-20 had a capacitance retention of 91 % after 10,000 cycles at 5 A g^{-1}. This is in contrast to its initial value, and the inset picture also shows the GCD curves of the first and the last cycles, which indicate that there is no obvious deformation.

The electrochemical performance and simulation of the actual device behavior of NPC-20 were further tested in a two-electrode system with identical amounts of active materials on both electrodes-illustrated in Fig. 5.5.

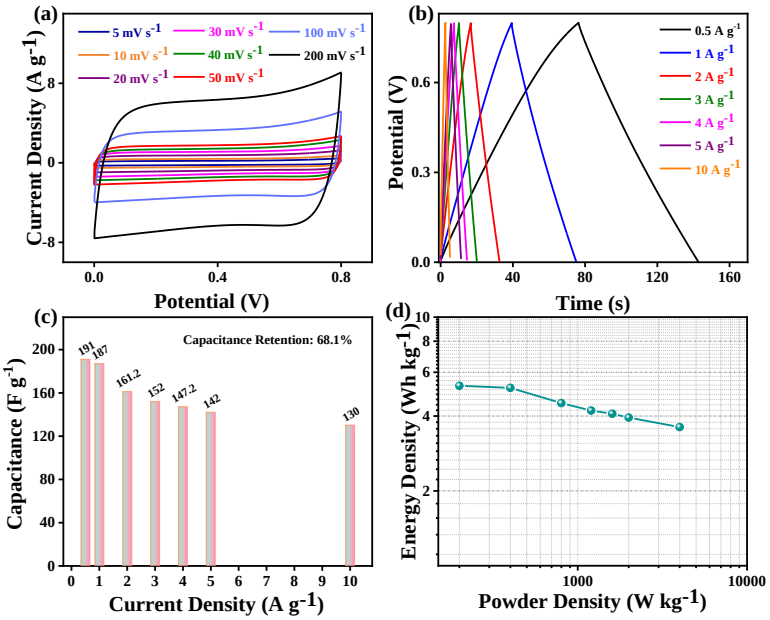

Fig. 5.5: (a, b) CV curves and GCD curves of HCNS-20 at a scan rate of 5-200 mV s^{-1} and an electric density of 0.5-10 A g^{-1}; (c) Specific capacitances at different current densities from 0.5 A g^{-1} to 10 A g^{-1}; (d) Ragone plots of NPC-20 in a two-electrode system

The CV curves of NPC-20 in Fig. 5.5a showed quasi-rectangular shapes with an increasing scan rate from 5 mV s^{-1} to 200 mV s^{-1}, indicating quick dynamics and good charge propagation. The GCD profiles of NPC-20 at various specific current values (0.5-10 A g^{-1}) were shown in Fig. 5.5b. All the GCD profiles display a quasi-symmetric triangular pattern, which suggests a superior charge-discharge reversibility and a good ability to store charge in the assembled symmetric supercapacitor. Fig. 5.5c showed the specific capacitance of the NPC-20 electrode at different specific currents, calculated from the GCD profiles. Obviously, the NPC-20 electrode possessed a capacitance retention of 68.1 % from 191 F g^{-1} to 130 F g^{-1}. Fig. 5.5d showed the Ragone plots of the NPC-20 electrodes in which the energy density and the power density were

calculated using the specific capacitance of the sample at a particular current density. The NPC-20 registered the maximum energy density as 5.3 Wh kg^{-1} at a power density of 0.2 kW kg^{-1} and showed maximum power density as 4 kW kg^{-1} at 3.6 Wh kg^{-1}, normalized by the total mass of the active materials.

5.4 Conclusion

In this study, N-doped porous carbon materials possessing a high SSA and appropriate N doping were successfully synthesized by a salt template-assisted monomer deposition method. NaCl was used as the salt template to create a porous structure for the NPC, the transition metal $Co(NO_3)_2$ $6H_2O$ induced monomer deposition, and 3-A as the carbon and nitrogen precursor led to hetero-atom doping in NPC. The dosage of NaCl had an effect on the surface area and pore volume of the NPC samples. The NPC-20 obtained exhibits the highest SSA and the largest total pore volume. As an electrode material for supercapacitors, it showed a high specific capacitance of 277 F g^{-1} at 1 A g^{-1} and excellent cycling stability, which was retained 91 % after 10,000 cycles. We expected that this simple and green route will enable a broader application in adsorption separation, energy storage, catalysis, and so on.

References

[1] Simon P, Gogotsi Y. Materials for electrochemical capacitors. Nature Materials. 2008, 7(11): 845-854.

[2] Zheng X, Luo J, Lv W, Wang D. W, and Yang Q. H. Two-dimensional porous carbon: Synthesis and ion-transport properties. Advanced Materials. 2015, 27(36): 5388-5395.

[3] Lv R, Robinson J A, Schaak R E, Sun D, and Terrones M. Transition metal dichalcogenides and beyond: Synthesis, properties, and applications of single- and few-layer nanosheets. Accounts of Chemical Research. 2015, 48(1): 56-64.

[4] Fan G, Li F, Evans D G, and Duan X. Catalytic applications of layered double hydroxides: Recent advances and perspectives. Chemical Society Reviews. 2014, 43(20): 7040-7066.

[5] Yan J, Ren C E, Maleski K, Hatter C B, Anasori B, Urbankowski P, Sarycheva A, and Gogotsi Y. Flexible MXene/graphene films for ultrafast supercapacitors with outstanding volumetric capacitance. Advanced Functional Materials. 2017, 27(30): 1701264.

[6] Bonaccorso F, Colombo L, Yu G, Stoller M, and Pellegrini V. Graphene, related two-dimensional crystals, and hybrid systems for energy conversion and storage. Science. 2015, 347(6217): 1246501.

[7] Lee J S, Kim S I, Yoon J C, and Jang JH. Chemical vapor deposition of mesoporous graphene nanoballs for supercapacitor. ACS Nano. 2013, 7(7): 6047-6055.

[8] Roberts A D, Li X, Zhang H. Porous carbon spheres and monoliths: Morphology

control, pore size tuning and their applications as Li-ion battery anode materials. Chemical Society Reviews. 2014, 43(13): 4341-4356.

[9] Veca L M, Meziani M J, Wang W, Wang X, Lu F, Zhang P, Lin Y, Fee R, Connell J W, and Sun Y P. Carbon nanosheets for polymeric nanocomposites with high thermal conductivity. Advanced Materials. 2009, 21(20): 2088-2092.

[10] Shen W, Hu T, Fan W. Cellulose generated-microporous carbon nanosheets with nitrogen doping. RSC Advances. 2014, 4(18): 9126-9132.

[11] Lu A H, Li W C, Schmidt W, and Schüth F. Fabrication of hierarchically structured carbon monoliths via self-binding and salt templating. Microporous and Mesoporous Materials, 2006, 95(1-3):187-192.

[12] Li N, Yang G, Sun Y, Song H，Cui H，Yang G，and Wang C. Free-standing and transparent graphene membrane of polyhedron box-shaped basic building units directly grown using a NaCl template for flexible transparent and stretchable solid-state supercapacitors. Nano Letters. 2015, 15(5): 3195-3203.

[13] Wang, H, Ding, Y, Nong, J, Pan Q，and Li Q. Bifunctional NaCl template for the synthesis of Si@graphitic carbon nanosheets as advanced anode materials for lithium ion batteries. New Journal of Chemistry, 2020, 44, 14278-14285.

[14] Liu T, Liu G. Block copolymer-based porous carbons for supercapacitors. Journal of Materials Chemistry. 2019, 7(41): 23476-23488.

[15] Lin T, Chen I. W, Liu F, Yang C，Bi H，Xu F，and Huang F. Nitrogen-doped mesoporous carbon of extraordinary capacitance for electrochemical energy storage. Science. 2015, 350: 1508-1513.

[16] Xu Z, Zhuang X, Yang C, Cao J，Yao Z，Tang Y，Jiang J，Wu D，and Feng X. Nitrogen-doped porous carbon superstructures derived from hierarchical assembly of polyimide nanosheets. Adv. Mater. 2016, 28, 1981-1987.

[17] Ding B, Guo D, Wang Y, Wu, X L，and Fan Z J. Functionalized graphene nanosheets decorated on carbon nanotubes networks for high performance supercapacitors[J]. Journal of Power Sources. 2018, 398: 113-119.

[18] Feng L X, Wang K, Zhang X, Sun X Z，Li C，Ge X B，and Ma Y W. Flexible solid-state supercapacitors with enhanced performance from hierarchically graphene nanocomposite electrodes and ionic liquid incorporated gel polymer electrolyte. Advanced Functional Materials. 2018, 28(4): 1704463.

[19] Zhao G，Chen C，Yu D，Sun L，Yang C，Zhang H，Sun Y，Besenbacher F, and Yu M. One-step production of ONS co-doped three-dimensional hierarchical porous carbons for high-performance supercapacitors. Nano Energy. 2018, 47: 547-555.

[20] Wang Y, Song Y, and Xia Y. Electrochemical capacitors: mechanism, materials, systems, characterization and applications. Chemical Society Reviews. 2016, 45(21): 5925-5950.

[21] Zhang N, Gao N, Fu C, Liu D，Li S，Jiang L，Zhou H，and Kuang Y. Hierarchical porous carbon spheres/graphene composite for supercapacitor with both aqueous solution and ionic liquid. Electrochimica Acta. 2017, 235: 340-347.

[22] Andreas H A. Self-discharge in electrochemical capacitors: A perspective article. Journal of the Electrochemical Society. 2015, 162(5).

[23] Zou K, Deng Y, Chen J, Qian Y，Yang Y，Li Y，and Chen G. Hierarchically porous nitrogen-doped carbon derived from the activation of agriculture waste by potassium hydroxide and urea for high-performance supercapacitors. Journal of Power Sources. 2018: 579-588.

[24] Zeng D, Dou Y, Li M, Zhou M，Li H，Jiang K，Yang F，and Peng J. Wool fiber-derived nitrogen-doped porous carbon prepared from molten salt carbonization method for supercapacitor application. Journal of Materials Science. 2018, 53(11): 8372-8384.

[25] Wu K, Gao B, Su J, Peng X，Zhang X，Fu J，Peng S，and Chu PK. Large and porous carbon sheets derived from water hyacinth for high-performance supercapacitors. RSC Advances. 2016, 6(36): 29996-30003.

[26] Liu H, Zhai D D, Wang M, Liu J S, Chen X Y, and Zhang Z J. Design of urea-modified phenol-formaldehyde as well as the derived N-carbon nanosheets for supercapacitors with elevated rate capability and cycling stability. ChemelectroChem. 2019, 6(3): 885-891.

[27] Du J, Liu R, Yu Y, Zhang Y，Zhang Y，and Chen A B. N-doped ordered mesoporous carbon prepared by solid-solid grinding for supercapacitors. Journal of Materials Research. 2018, 33(20): 3408-3417.

[28] Cheng Y L, Wu L L, Fang C Q, Li T H，Chen J, Yang M N, and Zhang Q L. Synthesis of porous carbon materials derived from laminaria japonica via simple carbonization and activation for supercapacitors. Journal of Materials Research and Technology. 2020, 9(3): 3261-3271.

[29] Sylla N F, Ndiaye N. M, Ngom B. D, Mutuma B K, Momodu D, Chaker M, and Manyala N. Ex-situ nitrogen-doped porous carbons as electrode materials for high performance supercapacitor. Journal of Colloid and Interface Science. 2020, 569: 332-345.

[30] Qiu B, Pan C T, Qian W J, Peng Y J, Qiu L H, and Yan F. Nitrogen-doped mesoporous carbons originated from ionic liquids as electrode materials for supercapacitors. Mater. Chem. 2013, 1(21): 6373-6378.

[31] Zhang Y X, Liu L, Zhang L L,Yu Y F, Lv H J, and Chen A B. Template-free method for fabricating carbon nanotube combined with thin N-doped porous carbon composite for supercapacitor. Journal of Materials ence, 2019, 54(8): 6451-6460.

[32] Xu G Y, Ding B, Nie P, Shen L F, Wang J, and Zhang X G. Porous nitrogen-doped carbon nanotubes derived from tubular polypyrrole for energy-storage applications. Chem.-A Eur. J. 2013, 19: 12306-12312.

[33] Liu X H, Zhou L, Zhao Y Q, Bian L, Feng X T, and Pu Q S. Hollow, spherical nitrogen-rich porous carbon shells obtained from a porous organic framework for the supercapacitor. ACS Appl. Mater. Interfaces. 2013, 5(20): 10280-10287.

[34] Wei T Y, Wei X L, Yang L W, Xiao H P, Gao Y, and Li H M. A one-step moderate-explosion assisted carbonization strategy to sulfur and nitrogen dual-doped porous carbon nanosheets derived from camellia petals for energy storage. Journal of Power Sources. 2016, 331: 373-381.

[35] Lin G X, Ma R G, Zhou Y, Liu Q, Dong X P, and Wang J C. KOH activation of biomass-derived nitrogen-doped carbons for supercapacitor and electrocatalytic

oxygen reduction. Electrochimica Acta. 2018, 261: 49-57.

[36] Liu B, Liu Y J, Chen H B, Yang M, and Li H M. Oxygen and nitrogen co-doped porous carbon nanosheets derived from Perilla frutescens for high volumetric performance supercapacitors. Journal of Power Sources. 2017, 341: 309-317.

[37] Dutta S, Bhaumik A, and Wu K C-W. Hierarchically porous carbon derived from polymers and biomass: effect of interconnected pores on energy applications. Energy and Environmental Science. 2014, 7(11): 3574-3592.

[38] Xu X T, Wang M, Liu Y, Li Y J, Lu T, and Pan L K. In situ construction of carbon nanotubes/nitrogen-doped carbon polyhedra hybrids for supercapacitors. Energy Storage Mater. 2016, 5: 132-138.

CHAPTER 6

Conclusions of the Dissertation

In this dissertation, the starting point is energy storage, environmental pollution and other issues, taking doped porous carbon materials as the research object, by studying the synthesis method, reaction conditions, and so on; in the process, the morphology control method was explored and nitrogen-doped carbon nanotubes and porous N-doped carbon nanosheets, respectively, were successfully prepared. The electrochemical performance of these materials for supercapacitors was also investigated in detail. And all of them exhibited outstanding electrochemical performance in supercapacitors.

First, nitrogen-doped porous carbon nanotubes with high SSA, high nitrogen content and plentiful porous structure were easily prepared by a process of mixed salts activation. In this section, we adopted PPy as the carbon and nitrogen precursor, mixed salts as the activation agent, to explore the affect of activation condition and the amount of reactant to the final production. The experiment result shows that the molar ratio of PPy to NaCl/$ZnCl_2$ and the carbonization temperature are effected the pore structure and the electrochemical performance of the porous carbon nanotubes. Under optimal activation condition, porous carbon nanotubes presented tubular morphology, high specific surface area and high N-doped. Electrochemical characterization demonstrated that the as obtained porous carbon nanotubes displayed outstanding electrochemical

performance than other carbon materials. This strategy avoids the use of organic solvents, easy operating, economical and scalable. We look forward to this study can provide a new idea for the synthesis of porous carbon nanotubes, and the synthesized materials are expected to be used in more fields.

Secondly, NaCl “salt templating” strategy were used to prepared N-doping porous carbon nanosheets. The heteroatom doping strategy can greatly improve the electrochemical performance of carbon materials. This section we used 3-A was the carbon and nitrogen precursor and $Co(NO_3)_2$ $6H_2O$ was the catalyst. By adjusting the mass ratio of template to 3-A to investigate the morphology, the pore structure, and the capacitive performance of the samples. Benefit by both porous architecture and the suitable nitrogen doping, the obtained NPC-20 exhibits excellent rate capability and high capacitance. The superior electrochemical performance indicated that the prepared NPC-20 also has great potential for application in other technological areas.